CRISPR-screen identifies ZIP9 and dysregulated Zn2+ homeostasis as a cause of cancer-associated changes in glycosylation

Romer, T.B.; Khoder-Agha, F.; Aasted, M.K.M.; Haan, N. de; Horn, S.; Dylander, A.; ... ; Wandall, H.H.

Glycobiology, 2023, **33**, 9, 700–714
https://doi.org/10.1093/glycob/cwad003
Advance access publication date 16 January 2023
Original Article

CRISPR-screen identifies ZIP9 and dysregulated Zn^{2+} homeostasis as a cause of cancer-associated changes in glycosylation

Troels Boldt Rømer[1,2], Fawzi Khoder-Agha[1], Mikkel Koed Møller Aasted[1], Noortje de Haan[1], Sabrina Horn[1], August Dylander[1], Tao Zhang[3], Emil Marek Heymans Pallesen, Sally Dabelsteen[1], Manfred Wuhrer[3], Christine Flodgaard Høgsbro[1], Emil Aagaard Thomsen[4], Jacob Giehm Mikkelsen[4], Hans H. Wandall[1,*]

[1]Copenhagen Center for Glycomics, Department of Cellular and Molecular Medicine, University of Copenhagen, Blegdamsvej 3B, 2200 Copenhagen, Denmark, [2]Department of Clinical Medicine, University of Copenhagen, Blegdamsvej 3B, 2200 Copenhagen, Denmark, [3]Center for Proteomics and Metabolomics, Leiden University Medical Center, Einthovenweg 20, 2333 ZC Leiden, Netherlands, [4]Department of Biomedicine, Aarhus University, Høegh-Guldbergs Gade 10, 8000 Aarhus, Denmark

*Corresponding author: Email: hhw@sund.ku.dk

Introduction: In epithelial cancers, truncated *O*-glycans, such as the Thomson-nouveau antigen (Tn) and its sialylated form (STn), are upregulated on the cell surface and associated with poor prognosis and immunological escape. Recent studies have shown that these carbohydrate epitopes facilitate cancer development and can be targeted therapeutically; however, the mechanism underpinning their expression remains unclear.
Methods: To identify genes directly influencing the expression of cancer-associated *O*-glycans, we conducted an unbiased, positive-selection, whole-genome CRISPR knockout-screen using monoclonal antibodies against Tn and STn.
Results and Conclusions: We show that knockout of the Zn^{2+}-transporter *SLC39A9* (ZIP9), alongside the well-described targets *C1GALT1* (C1GalT1) and its molecular chaperone, *C1GALT1C1* (COSMC), results in surface-expression of cancer-associated *O*-glycans. No other gene perturbations were found to reliably induce *O*-glycan truncation. We furthermore show that ZIP9 knockout affects *N*-linked glycosylation, resulting in upregulation of oligo-mannose, hybrid-type, and α2,6-sialylated structures as well as downregulation of tri- and tetra-antennary structures. Finally, we demonstrate that accumulation of Zn^{2+} in the secretory pathway coincides with cell-surface presentation of truncated *O*-glycans in cancer tissue, and that over-expression of COSMC mitigates such changes. Collectively, the findings show that dysregulation of ZIP9 and Zn^{2+} induces cancer-like glycosylation on the cell surface by affecting the glycosylation machinery.

Key words: cancer antigens; CRISPR screen; SLC39A9; Tn; zinc homeostasis.

Introduction

The attachment of glycans to proteins, known as glycosylation, is the most abundant and diverse post-translational modification known (Varki et al. 2015), and changes in glycosylation is a common feature in most cancer cells (Julien et al. 2012; Stowell et al. 2015; Chia et al. 2016). Mucin-type O-GalNAc-glycans (hereafter referred to as *O*-glycans) are found on 85% of all secreted or surface-expressed proteins (Steentoft et al. 2013; King et al. 2017). A well-known alteration in cancers is the shortening of *O*-glycans, resulting in surface-expression of the truncated *O*-glycan antigens Tn (Thomsen-nouveau antigen; GalNAcα-Ser/Thr) and its sialylated derivative, STn (sialyl-Tn, CD175; NeuAc2,6GalNAcα-Ser/Thr; Rømer et al. 2021).

Tn and STn are highly expressed in a large proportion of epithelial cancers. Tn is e.g. surface-expressed in >20% of breast cancers and not in healthy tissue, whereas STn is found in >80% of colorectal cancers and very rarely in healthy tissue (Springer 1983, 1984; Cervoni et al. 2020; Rømer et al. 2021). Expression of truncated *O*-glycans has been shown to promote invasiveness, drive tumor formation, affect immune function, and correlate with poor clinical outcome (Coon et al. 1982; Springer 1984; Kobayashi et al. 1992; Werther et al. 1996; Springer 1997; Desai 2000; van Vliet et al. 2006; Madsen et al. 2012; Madsen et al. 2013; Radhakrishnan et al. 2014; Gao et al. 2016). These features make Tn and STn attractive targets in immunotherapies and several antibody-based treatments are currently entering clinical trials (Pinho and Reis 2015; Posey et al. 2016; Steentoft et al. 2018; Mereiter et al. 2019). In addition to changes in *O*-glycosylation, other glycan types are also affected in cancers. For example, a global increase in sialylation of *N*-glycans as well as a shift from α2,3-linked sialylation to α2,6-linked sialylation has been identified in several types of cancer and contribute to tumor growth and metastasis (Büll et al. 2014). Likewise, changes in *N*-linked glycans—including increased expression of both oligo-mannose and hybrid *N*-glycans—are observed in tumors and associated with metastasis (Dennis et al. 1987).

Despite the clinical relevance of truncated *O*-glycans, our understanding of the mechanisms driving the expression of Tn and STn in cancers remains incomplete, making it

Received: July 27, 2022. **Revised:** January 2, 2023. **Accepted:** January 2, 2023

difficult to manipulate *O*-glycan presentation or predict escape mechanisms in a clinical setting. The Tn-antigen is synthesized as an intermediate in the secretory pathway when 1 of 20 enzymes belonging to the GalNAc-transferase (GalNAc-T) family catalyzes the attachment of *N*-acetylgalactosamine (GalNAc) to serine, threonine, or tyrosine residues (Fig. 1a; Bennett et al. 2012; Brockhausen and Stanley 2015; Wandall et al. 2021). The sialyltransferase ST6GALNAC1 can further cap Tn with a sialic acid in an α2,6-linkage to form STn. In healthy tissue, the enzyme C1GalT1 (T-Synthase/core 1 β3-galactosyltransferase, encoded by *C1GALT1*) instead elongates Tn with a galactose residue, forming the T-structure (core 1; Ju and Cummings 2014: 1). Several mechanisms that could disrupt this delicate biosynthetic process have been suggested to drive surface-expression of Tn and STn. Among these, dysregulation and loss of function mutations of the molecular chaperone to the C1GalT1 enzyme COSMC (core 1 β3-Galactosyltransferase-Specific Molecular Chaperone, encoded by *C1GALT1C1*) has been among the most prominent (Ju and Cummings 2002; Wang et al. 2010; Ju et al. 2014). However, although some cancers exhibit silencing of or mutations in *C1GALT1C1*, not all Tn-positive cancers show downregulation of COSMC or C1GalT1 (Schietinger et al. 2006; Ju et al. 2008; Radhakrishnan et al. 2014; Sun et al. 2018). An alternative theory is that pH changes (Axelsson et al. 2001; Hassinen et al. 2011), or relocation of GalNAc-Ts in the secretory pathway, drives Tn- and STn-expression (Gill et al. 2010; Nguyen et al. 2017). These hypotheses are not mutually exclusive and although they might, individually or combined, explain Tn- and STn-expression in a subset of cancers, a full understanding of the mechanisms driving truncation of *O*-glycans in cancers is still lacking.

Advances in the CRISPR/Cas9-technology has accelerated research in functional genomics and the use of high-throughput forward genetics screens for diverse applications (Zhou et al. 2014; DeNicola et al. 2015; Han et al. 2018). Whole-genome CRISPR knockout screens enable the parallel perturbation of all genes in the human genome and by enriching or depleting a certain subpopulation of mutant cells, genes essential to e.g. antigen presentation, toxin resistance, or viral infections can be identified (Shalem et al. 2014). The technology has been shown to outperform RNA interference (RNAi) screens with a higher signal-to-noise ratio, fewer off-target effects, and higher reproducibility (Evers et al. 2016; Housden and Perrimon 2016).

In this study, we conducted an antibody-based, positive-selection, whole-genome CRISPR knockout screen to identify genes linked to expression of the truncated, cancer-associated *O*-glycans Tn and STn. Our screen identified knockout of the gene *SLC39A9,* alongside *C1GALT1C1* and *C1GALT1*, to induce expression of truncated *O*-glycans with a high signal-to-noise ratio. No other gene targets that were significant across multiple single guide RNAs (sgRNAs) were identified. *SLC39A9* encodes a zinc-transporter, ZIP9, residing in the secretory pathway and we demonstrated that knockout of ZIP9 affects *O*-glycosylation as well as *N*-glycosylation. ZIP9 knockout results in accumulation of Zn^{2+} in the secretory pathway and we show that increased Zn^{2+}-concentrations directly induces expression of truncated *O*-glycans in vitro and that zinc accumulation and expression of truncated *O*-glycans coincide in tumors. Furthermore, we demonstrated that ZIP9 knockout results in downregulation of C1GalT1, which could be rescued by COSMC over-expression. Taken together, these findings show that dysregulation of Zn^{2+} induce alterations in the global biosynthesis of glycans. Most pronounced were the effects on protein *O*-glycans, exhibiting a cancer-like glycosylation on the cell surface, but changes in *N*-glycosylation were also induced, showing less extended glycan structures and an increase in sialylation, mostly pronounced α2,6 sialylation, whereas the effect on glycosphingolipids (GSL) was limited to a reduction of terminal fucose residues.

Results

CRISPR screen identifies *SLC39A9, C1GALT1,* and *C1GALT1C1* knockout to induce Tn and STn surface-expression

We conducted a positive-selection CRISPR/Cas9 whole-genome screen to identify genes that, when knocked out, induce expression of the antigens Tn and/or STn (Fig. 1b). The screen was conducted in the HaCaT keratinocyte cell line that we previously used to generate knockout cell lines, including cell lines lacking *C1GALT1C1* (Radhakrishnan et al. 2014). Initially, we established a HaCaT line (1B6B) with constitutive expression of Cas9 and blasticidin resistance using lentiviral transduction and evaluated Cas9 function using the IDAA (Indel Detection by Amplicon Analysis) technology (Supplementary Fig. 1a, see online supplementary material for a color version of this figure; Lonowski et al. 2017). We further secured that Cas9 expression did not induce Tn-expression (Supplementary Fig. 1b, see online supplementary material for a color version of this figure) and demonstrated that we could isolate Tn-positive HaCaT deficient in COSMC using fluorescence-activated cell sorting (FACS; Supplementary Fig. 1c, see online supplementary material for a color version of this figure). HaCaT 1B6B cells were subsequently transduced with the Brunello library targeting 19,114 genes with 4 guides per gene and 1,000 nontargeting guides (a total of 77,441 guides) to create a mutant cell pool (Doench et al. 2016). Using FACS and a mix of the well-characterized, monoclonal antibodies 5F4 (anti-Tn) and 3F1 (anti-STn), we enriched the mutant cell pool for both Tn- and STn-positive cells (Mandel et al. 1991; Thurnher et al. 1993). Transduction with the genome-wide library induced Tn- and/or STn-expression in 0.05% of the cells as evaluated by FACS. After expanding the Tn/STn-positive cells, we repeated FACS using either 5F4 or 3F1, enriching for Tn- or STn-positive cells, respectively. We used high-throughput next generation sequencing (NGS) to determine the presence of sgRNAs in the Tn/STn-negative population after the first FACS and in the Tn- positive and STn-positive cell populations after the second FACS. In the negative sample, sgRNAs were identified targeting all but 2 genes (*PSMA7* and *RRM1*), yielding a coverage of 99.99% of the 19,114 genes targeted in the Brunello library with a Gini-coefficient of the distribution of sgRNA of 0.296 (Supplementary Fig. 2).

Our screen identified 3 strong gene hits (*SLC39A9*, *C1GALT1*, and *C1GALT1C1)* that were significantly targeted with multiple sgRNAs and enriched in both the Tn-positive and the STn-positive populations (Fig. 1c, Supplementary Table III). *SLC39A9* encodes a zinc-transporter, ZIP9, thought to reside in the secretory pathway, namely in the Golgi apparatus, with steroid receptor function (Matsuura et al. 2009; Thomas et al. 2014, 2018: 9). *C1GALT1* encodes the enzyme C1GalT1, known to elongate the Tn-antigen, and *C1GALTC1* encodes its molecular chaperone, COSMC. Remarkably, no other genes came out with significant gene

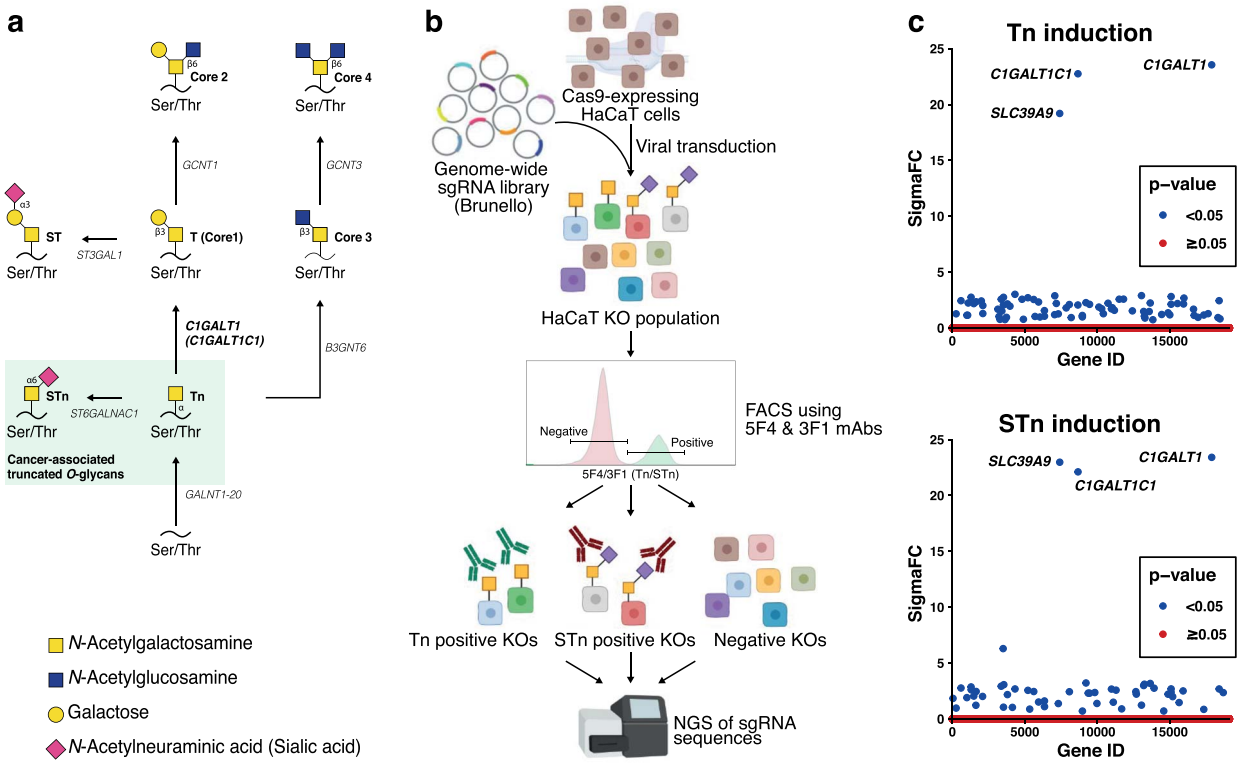

Fig. 1. CRISPR-mediated whole-genome screen using antibodies against Tn and STn identifies ZIP9 knockout to induce truncated *O*-glycans. a) Schematic overview of the *O*-GalNAc glycan biosynthetic pathway, focusing on the synthesis of Tn, core 1, core 2, core 3, and core 4 structures. Glycan structures are represented by the SNFG, where: yellow square: *N*-acetylgalactosamine; blue square: *N*-acetylglucosamine; yellow circle: galactose; and pink diamond: *N*-acetylneuraminic acid. b) Illustration of overall experimental strategy. HaCaT 1B6B cell line with constitutive Cas9-expression was transduced with a lentiviral preparation of the Brunello library resulting in a cell population with knockout clones representing all targeted genes in the genome. A first round of FACS using a mixture of antibodies against Tn (green) and STn (red) separated knockouts with truncated *O*-glycans and without. A second round of FACS using antibodies against only Tn or STn enriched and separated clones further. c) Graphic depiction of gene ranking for Tn- (top) and STn-positive (bottom) knockouts, based on SigmaFc score calculated using the PinAPL-Py software. Statistically significant genes ($P < 0.05$) are displayed in blue, insignificant genes ($P \geq 0.05$) are shown in red.

scores across multiple sgRNAs and all other identified targets varied across replicates, suggesting that, under these experimental conditions, only knockout of *SLC39A9*, *C1GALT1*, and *C1GALT1C1* resulted in truncation of O-glycans.

To perform target validation, we used CRISPR/Cas9 to knockout ZIP9 in the HaCaT cell line and the more differentiated N/TERT-1 keratinocyte cell line. In both HaCaT and N/TERT-1 cells, we found that knockout of ZIP9 yielded surface-expression of Tn and STn, as evaluated by immunofluorescent microscopy on nonpermeabilized cells using the 5F4 and 3F1 antibodies (Fig. 2a and b). Surface-expression was verified using flow cytometry, staining with 5F4 (Fig. 2c and d). Pretreating the cells with neuraminidase to convert STn to Tn resulted in an increased staining intensity (Supplementary Fig. 3a and b, see online supplementary material for a color version of this figure). Despite expression of Tn and STn, we found no decrease in surface-localized T-antigen when staining with PNA lectin or 3C9 antibody (Fig. 2c and d, Supplementary Fig. 3c, see online supplementary material for a color version of this figure).

Knockout of ZIP9 affects *O*-, *N*-, and GSL-glycosylation

We next performed mass spectrometry (MS)-based glycoprofiling of N/TERT-1 ZIP9 knockout cells. For O-glycans, we confirmed that the relative Tn-expression increased 7–8-fold in ZIP9 knockout cells as compared with wildtype cells (Fig. 3, Supplementary Table IV). Interestingly, the total level of core 1 *O*-glycans was not affected by ZIP9 knockout (Fig. 3, Supplementary Table IV), whereas we observed a slight decrease in surface-exposed core 1 using flow cytometry with the PNA lectin and the 3C9 antibody, both of which bind core 1 structure (Fig. 2c and d, Supplementary Fig. 3c). On the contrary, core 2 O-glycans were diminished in ZIP9-deficient cells to almost nondetectable levels, while accounting for >30% of the O-glycans in wildtype cells (Fig. 3, Supplementary Table IV). Finally, core 3 structures accounted for <5% of the O-glycans in N/TERT-1 wildtype cells and this level appeared to be only slightly lower upon knockout of ZIP9. Of note, RT-qPCR analysis of *ZIP9* knockout N/TERT-1 cells revealed no alterations in transcription of *C1GALT1*, *C1GALT1C1*, or *GNCT1*, responsible for the core 1 and core 2 structures, respectively (Supplementary Fig. 4, see online supplementary material for a color version of this figure). The transcription of *ST6GALNAC1*, responsible for formation of the STn-antigen, was likewise not altered in ZIP9 knockout N/TERT-1 cells.

For *N*-glycans, the level of tri- and tetra-antennary glycans as well as the abundance of di-antennary glycans carrying LacDiNAc (GalNAcβ1,4-GlcNAc) was decreased in knockout cells as compared with wildtype, of which the first was confirmed by weaker staining with the L-PHA lectin (Fig. 4a and d, Supplementary Fig. 3d, see online supplementary material for a color version of this figure, Supplementary Table IV). Furthermore, we observed an increase in the relative abundance of hybrid-type *N*-glycans in the ZIP9 knockout cells as compared with wildtype,

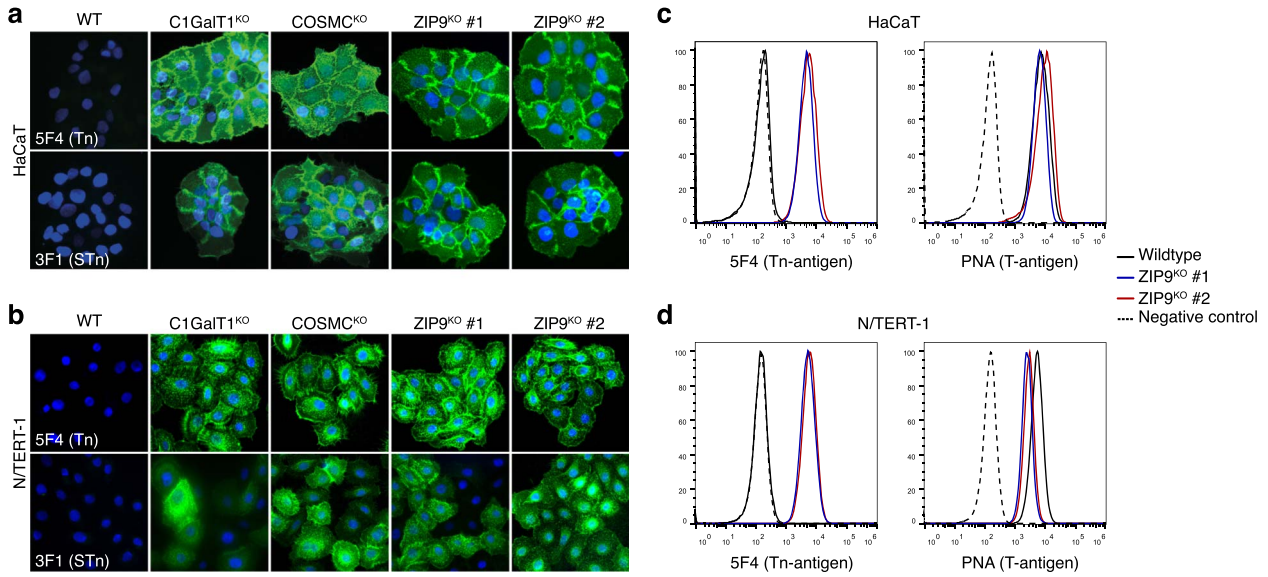

Fig. 2. Validation of Tn/STn-inducing knockouts and the effect of zinc in regulation of Tn-expression. a,b) Immunostaining of HaCaT and N/TERT-1 wildtype (WT) or stable *C1GALT1* (C1GalT1), *C1GALT1C1* (COSMC), or 2 separate *SLC39A9* (ZIP9) knockout cells for validation of their expression of Tn and STn using the monoclonal 5F4 and 3F1 antibodies. c,d) Histograms showing flow cytometry fluorescent intensity of 10,000 viable HaCaT and N/TERT-1 wildtype (solid black) or 2 separate ZIP9 knockout cells (blue and red) stained with the 5F4 monoclonal antibody or the PNA lectin, respectively. Wildtype cells stained only with secondary antibodies were used as a negative control (dashed black).

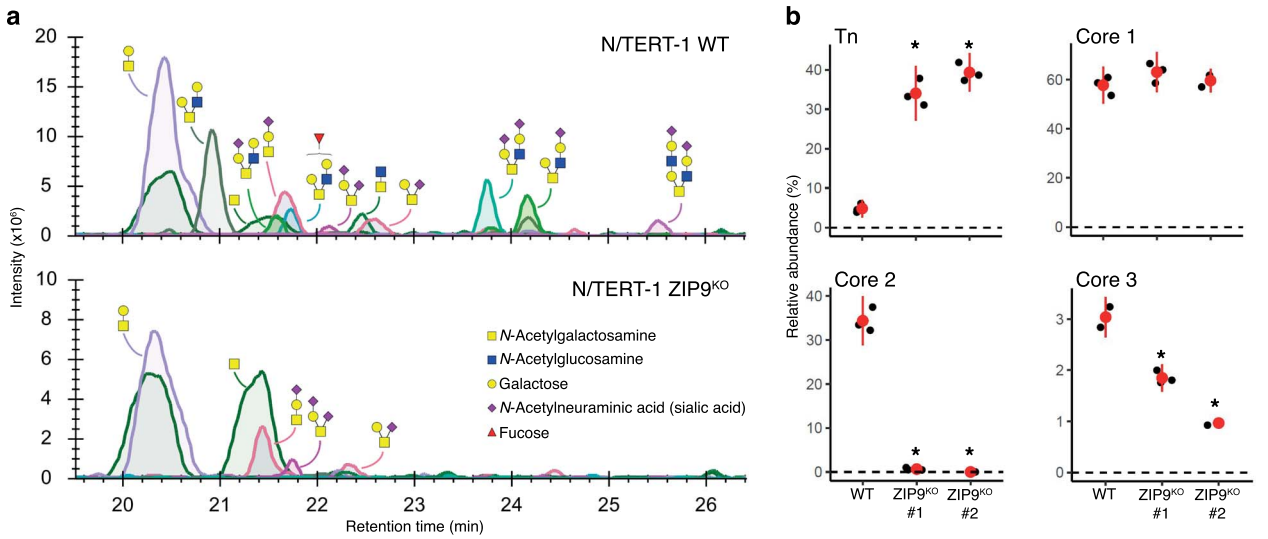

Fig. 3. MS-based *O*-glycan profiling of N/TERT-1 ZIP9 knockout lysates. a) Representative data from the *O*-glycan profiling of N/TERT-1 wildtype (top) and ZIP9 knockout (bottom) lysates, showing the extracted ion chromatograms of the 12 most abundant *O*-GalNAc type glycans. The annotated structures are based on previous assignments using glycan standards and MS/MS analysis. Unannotated signals correspond to other types of *O*-glycans that are isomeric to the annotated *O*-GalNAc glycans. b) Relative quantification of the 4 main *O*-GalNAc glycan cores: Tn, core 1, core 2, and core 3 in 3 technical replicates of one N/TERT-1 wildtype and 2 ZIP9 knockout clones. Black dots represent individual measurements, whereas red dots and vertical lines indicate the average and standard deviation of the replicates, respectively. Black asterisk: corrected *P*-value of *t*-test between knockout and wildtype < 0.05. Glycan structures are represented by the SNFG, where: yellow square: *N*-acetylgalactosamine; blue square: *N*-acetylglucosamine; yellow circle: galactose; pink diamond: *N*-acetylneuraminic acid; red triangle: fucose.

which was mainly driven by the increase of α2,6-sialylated structures (Fig. 4a and e, Supplementary Table IV). In general, we observed an increase in the average number of sialic acids per *N*-glycan for both complex- and hybrid-type *N*-glycans (Fig. 4e, Supplementary Table IV) in ZIP9-deficient cells. For complex-type *N*-glycans both α2,6- and α2,3-sialylation increased, but the increase was more pronounced for α2,6-sialylation (Fig. 4e, Supplementary Table IV). On the hybrid-type *N*-glycans, exclusively α2,6-sialylation was affected. The increase in surface sialylation was confirmed by increased staining with MAL-II and SNA lectins in ZIP9-deficient cells (Supplementary Fig. 3e and f), but RT-qPCR analysis did not detect consistent up- or downregulation of sialyltransferases at mRNA-level (Supplementary Fig. 4, see online supplementary material for a color version of this figure).

Analysis of GSL-glycans revealed gangliosides and linear neolacto-series to be the major GSL types in N/TERT-1 cells.

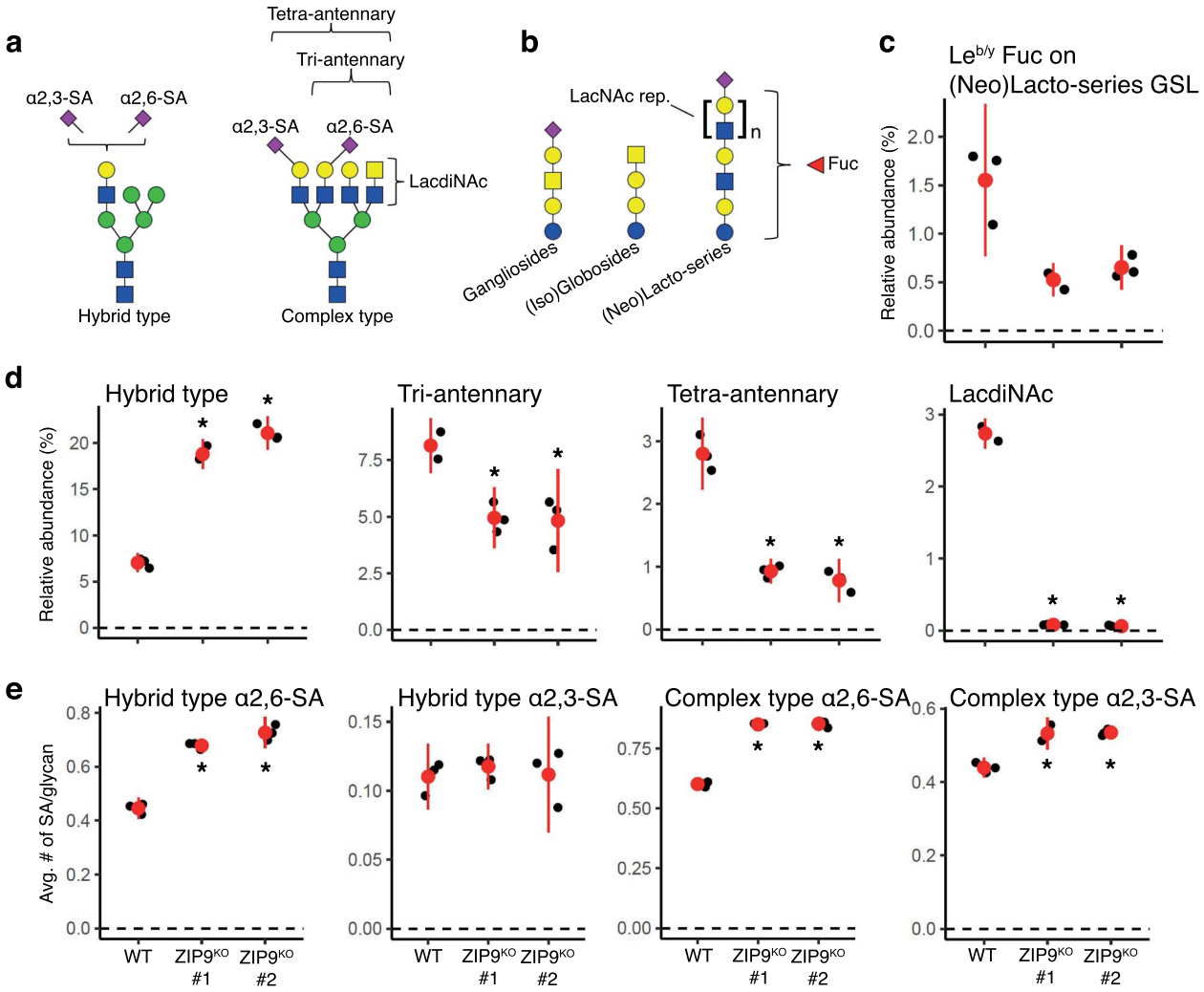

Fig. 4. MS-based *N*-glycan and GSL-glycan profiling of N/TERT-1 ZIP9 knockout lysates. a) Schematic representation of relevant *N*-glycan structural features and their nomenclature. b) Schematic representation of relevant GSL-glycan structural features and their nomenclature. Glycan structures are represented by the SNFG, where: yellow square: *N*-acetylgalactosamine; blue square: *N*-acetylglucosamine; yellow circle: galactose; green circle: Mannose; blue circle: glucose; pink diamond: *N*-acetylneuraminic acid (SA); and red triangle: Fucose. c) Relative quantification of GSL neolacto-series *N*-acetylglucosamine-linked fucosylation in 3 technical replicates of one N/TERT-1 wildtype and 2 ZIP9 knockout clones. d) Relative quantification of the structural *N*-glycan types and features: hybrid-type, tri-antennary complex-type, tetra-antennary complex-type, and LacdiNAc motives. e) Average number of α2,3- or α2,6-linked SAs per glycan for hybrid-type and complex-type *N*-glycans. Black dots represent individual measurements, whereas red dots and vertical lines indicate the average and standard deviation of the replicates, respectively. Black asterisk: Corrected *P*-value of *t*-test between knockout and wildtype < 0.05.

Therefore, we observed only minor changes upon knockout of ZIP9, the most pronounced one being the downregulation of neolacto-series' Lewis y or b structures (Fig. 4c).

ZIP9 knockout affects C1GalT1 expression in a COSMC dependent manner, but not secretory pathway morphology

As increased Tn-expression could be linked to decreased expression of the enzyme C1GalT1, we probed its expression in ZIP9-deficient cells. We observed a decrease in C1GalT1 expression in knockout cells but not a complete loss as evaluated by immunolabeling (Fig. 5a and c). This finding is in accordance with the increase in Tn on the cell surface and the simultaneous preservation of core 1 structures. To investigate if the downregulation of C1GalT1 is due to dysregulation of its chaperone COSMC, and to examine whether the zinc-binding domain of COSMC might play a role, we overexpressed COSMC wildtype and an E152K mutant suggested to be involved in Zn^{2+}-binding (Hanes et al. 2017), in ZIP9 deficient HaCaT cells. We observed almost a complete rescue of the C1GalT1 levels (Fig. 5e) and of the glyco-phenotype manifested by a 3-fold decrease in Tn-expression, using both the wildtype and mutant COSMC constructs (Fig. 5f and g). No significant changes were detected in T-antigen levels (Supplementary Fig. 5, see online supplementary material for a color version of this figure). To determine whether the effects seen on *N*-linked glycans, such as increased hybrid structures, are caused by a similar mechanism, we evaluated the expression levels of α-mannosidase II by immunolabeling and RT-qPCR but no significant change was detected (Fig. 5b and d, Supplementary Fig. 4, see online supplementary material for a color version of this figure).

Furthermore, we wanted to verify whether ZIP9 deficiency generally affects secretory pathway morphology. Fluorescent staining of different secretory pathway markers such as ER, Golgi, and endo-lysosomal markers for the most part showed

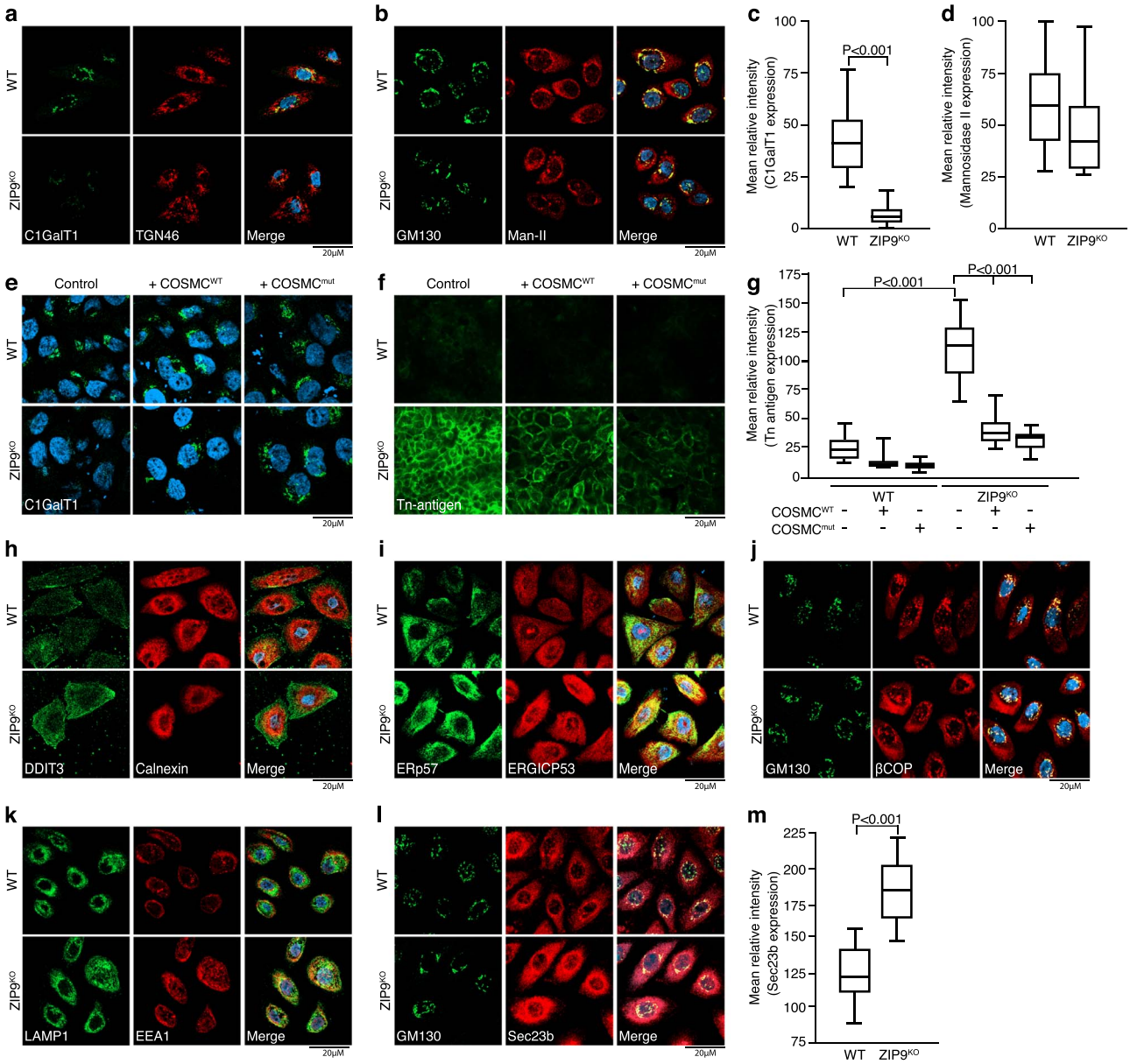

Fig. 5. Characterization of the secretory pathway of ZIP9 knockout cells. a) Immunostaining of C1GalT1. C1GalT1 (green) co-stained with Golgi marker TGN46 (red) and nucleus (DAPI blue) in wildtype and ZIP9 knockout N/TERT-1 cells. b) Immunostaining of mannosidase II. Man-II (red) co-stained with Golgi marker GM130 (green) and nucleus (DAPI blue) in wildtype and ZIP9 knockout N/TERT-1 cells. c) C1GalT1 expression was quantified, and mean intensity calculated in Zen Blue (n = 20–50 cells/group). d) Man-II expression was quantified, and mean intensity was calculated in Zen Blue (n = 20–50 cells/group). e) Wildtype and ZIP9 knockout HaCaT cells were transfected with COSMC wildtype or COSMC carrying a mutation in its zinc-binding site. C1GalT1 (green) was co-stained with nucleus (DAPI blue) in the transfected wildtype and ZIP9 knockout HaCaT cells. f) Wildtype and ZIP9 knockout HaCaT cells were transfected with COSMC wildtype or COSMC carrying a mutation in its zinc-binding site. Tn antigen (green) was stained with biotinylated lectin VVA. g) Tn expressions were quantified and calculated in Zen Blue (n = 20–50 cells/group). h–l) Secretory pathway markers were co-immunostained. m) Sec23b (red) expression levels in (l) were calculated and quantified in Zen Blue (n = 20–50 cells/group).

no visible changes in expression or location (Fig. 5h–l). Of note, the expression level of the member of the COPII complex, Sec23b, was significantly increased in ZIP9 knockout cells (Fig. 5l and m), which suggests an upregulation of anterograde vesicular trafficking in the knockout cells.

ZIP9 knockout increases Zn^{2+} in the secretory pathway and increased Zn^{2+} affects Tn-expression

ZIP9 is localized to the secretory pathway, having been identified in perinuclear compartments and co-localized with the trans Golgi network marker TGN58 (Matsuura et al. 2009; Thomas et al. 2014, 2018). In addition, ZIP9 have been shown to strongly co-localize with lysosomal and Golgi markers in HaCaT cells (Qiu et al. 2020: 9). ZIP9 serves as an efflux transporter, exporting zinc from the secretory pathway to the cytoplasm and coordinating with zinc importers (ZnTs) to maintain zinc homeostasis within the cell (Matsuura et al. 2009: 39; Thomas et al. 2014, 2018: 9). Therefore, we hypothesized that knockout of ZIP9 would lead to zinc accumulation in the secretory pathway, which could influence the general ion homeostasis and in turn the glycosylation outcome. To confirm this claim we used ZinPyr-1 as a Zn^{2+} fluorogenic reporter. As expected, N/TERT-1 ZIP9

knockout cells showed a significant increase in fluorescence when compared with wildtype cells, indicating an accumulation of zinc in the secretory pathway (Fig. 6a and b). To test whether altered Zn^{2+} concentration in the extracellular milieu affected the expression of truncated *O*-glycans, we titrated Zn^{2+} to the extracellular milieu of N/TERT-1 cells using $ZnCl_2$ and found a dose–response relationship between the number of Tn-positive cells and $ZnCl_2$ concentrations as evaluated by flow cytometry, accompanied by a gradual disorganization and re-localization of C1GalT1 and TGN46 (Fig. 6c and d). At $ZnCl_2$ concentrations of 100 μM, ~60% of the cells were Tn-positive, whereas 100% of the cells were positive at 125 μM. Likewise, C1GalT1 and TGN46 appeared to be progressively spread more throughout the cell with increasing $ZnCl_2$ concentrations. Notably, at these concentrations, cell viability was not affected, although higher concentrations of zinc began to decrease viability. Increasing extracellular concentrations of calcium and magnesium did not induce Tn surface-expression, whereas manganese induced a slight expression of Tn-antigen but also markedly decreased cell viability (Fig. 6d). To examine if accumulated Zn^{2+} coincides with the expression of truncated *O*-glycans in cancer tissue, we labeled frozen sections of human oral squamous cell carcinomas with the Zn^{2+} fluorogenic reporter, ZinPyr-1, and evaluated the co-expression of truncated *O*-glycans. Although it was not possible to perform a classical co-labeling due to the soluble nature of the Zn^{2+} probe, the labeling of serial sections strongly suggested that areas with high accumulation of signal from the Zn^{2+} probe coincided with the localization of Tn-expression (Fig. 6e).

Discussion

Using an unbiased, whole-genome CRISPR knockout screen coupled with an antibody-based, positive-selection strategy, we identified *SLC39A9* (ZIP9), *C1GALT1* (C1GalT1), and *C1GALT1C1* (COSMC) as the only genes that, when knocked out individually, induce surface-expression of the cancer-associated, truncated *O*-glycans Tn and STn.

Focusing on ZIP9, we showed that knockout of ZIP9 induces a cancer-like glyco-phenotype including surface-expression of truncated *O*-glycans and an increase in *N*-glycan sialylation. We demonstrated that ZIP9 knockout results in accumulation of Zn^{2+} in the secretory pathway and that increasing Zn^{2+} independent of ZIP9 knockout results in expression of truncated *O*-glycans. In agreement with this, we found that accumulation of zinc in tumor sections co-localized with Tn-expression. In addition, ZIP9 knockout results in downregulation of C1GalT1, which can be rescued by over-expression of COSMC. Over-expression of COSMC also rescues *O*-glycan truncation in ZIP9-deficient cells.

CRISPR screens enable identification of genes linked to a certain phenotype at a whole-genome level in a reliable and versatile manner. We utilized the widely used genome-wide Brunello library and subjected cells to stringent selection by FACS. Remarkably, there was a high signal-to-noise ratio in the screen. The 3 genes identified to induce Tn and STn surface-expression upon knockout (*SLC39A9*, *C1GALT1*, and *C1GALT1C1*) had 6- to 8-fold higher SigmaFC scores than the fourth and fifth most significant genes identified in the Tn and STn screens (Supplementary Table III). The SigmaFC gene score is calculated by addition of the fold changes of all sgRNAs multiplied by the number of sgRNAs that show significant enrichment. The higher SigmaFC scores for *SLC39A9*, *C1GALT1*, and *C1GALT1C1* was therefore primarily due to multiple sgRNAs that significantly induced Tn or STn-expression. This suggests that under the experimental conditions used, loss of only the 3 identified genes, and no other genes in the genome, led to induction of Tn or STn surface-expression. However, it cannot be ruled out that other genes might be involved in the regulation of truncated *O*-glycan expression in other cell types than skin keratinocytes. Furthermore, positive gene regulation might be able to induce Tn or STn as well, which could be assayed in a future gene activation screen (CRISPRa) or in a CRISPR knockout screen investigating reduction of Tn/STn-expression in Tn/STn-positive cancer cell lines. Importantly, knockout of ZIP9 in HEK293 cells by our colleagues also induced expression of Tn-antigen, indicating that this effect is not exclusive to keratinocytes (unpublished data).

ZIP9 encodes a zinc-transporter possessing membrane androgen receptor activity, and represents the only zinc-transporter known to function as a hormone receptor (Matsuura et al. 2009; Thomas et al. 2014, 2018: 9; Converse and Thomas 2020). The identification of ZIP9 as a regulator of glycosylation agrees with previous findings utilizing the subtilase toxin and a CRISPR screen to enrich for cells deficient in glycosylation (Yamaji et al. 2019). Interestingly, knockout of ZIP9 induces a glyco-phenotype that to a large extent resembles glycan structures often found in cancerous tissue. Most obvious is the increase in surface-expression of Tn and STn, which we confirm by both MS, lectin and antibody staining. Tn and STn have been known to be cancer-associated for 6 decades and are found in a range of epithelial tumors, but not in healthy tissue or tumors of nonepithelial origin (Springer 1983, 1984; Stowell et al. 2015; Cervoni et al. 2020; Rømer et al. 2021). We also observe a significant increase in global sialylation of *N*-glycans through both MS and lectin staining. Both the expression of Tn, STn, and the more general increased expression of especially 2,6 linked sialic acids on *N*-linked glycans are known to induce immune-tolerance through interactions with the C-type lectin MGL and members of the family of Siglecs (van Vliet et al. 2006; Crocker et al. 2007; Mathiesen et al. 2018; Chiodo et al. 2021). Accordingly, increased expression of Tn and sialylation in tumors has been shown to induce immune escape, metastasis, and tumor formation (Büll et al. 2014; Ju et al. 2014; Radhakrishnan et al. 2014; Bhide and Colley 2017). Oligo- mannose and hybrid *N*-glycans were also increased, which has previously been reported in e.g. colorectal cancers (Park et al. 2020; Boyaval et al. 2021). On the contrary, we also observed a downregulation of tri- and tetra-anterrary *N*-glycans, and GSL-profiling revealed a downregulation of Lewis b/y structures. In some cancers, such structures are upregulated and known to facilitate metastatic spread of tumor cells (Mehta et al. 2012; Blanas et al. 2018; de Vroome et al. 2018; Doherty et al. 2018; Hanzawa et al. 2022). However, although such branched and elongated structures are indeed upregulated at certain stages of tumor development, other structures, such as the identified Tn and STn *O*-glycans and the oligo-mannose and hybrid-type *N*-linked glycans, may dominate at different stages of tumor development.

The mechanism by which ZIP9 affects glycosylation is only explained in part by the findings in this study. The

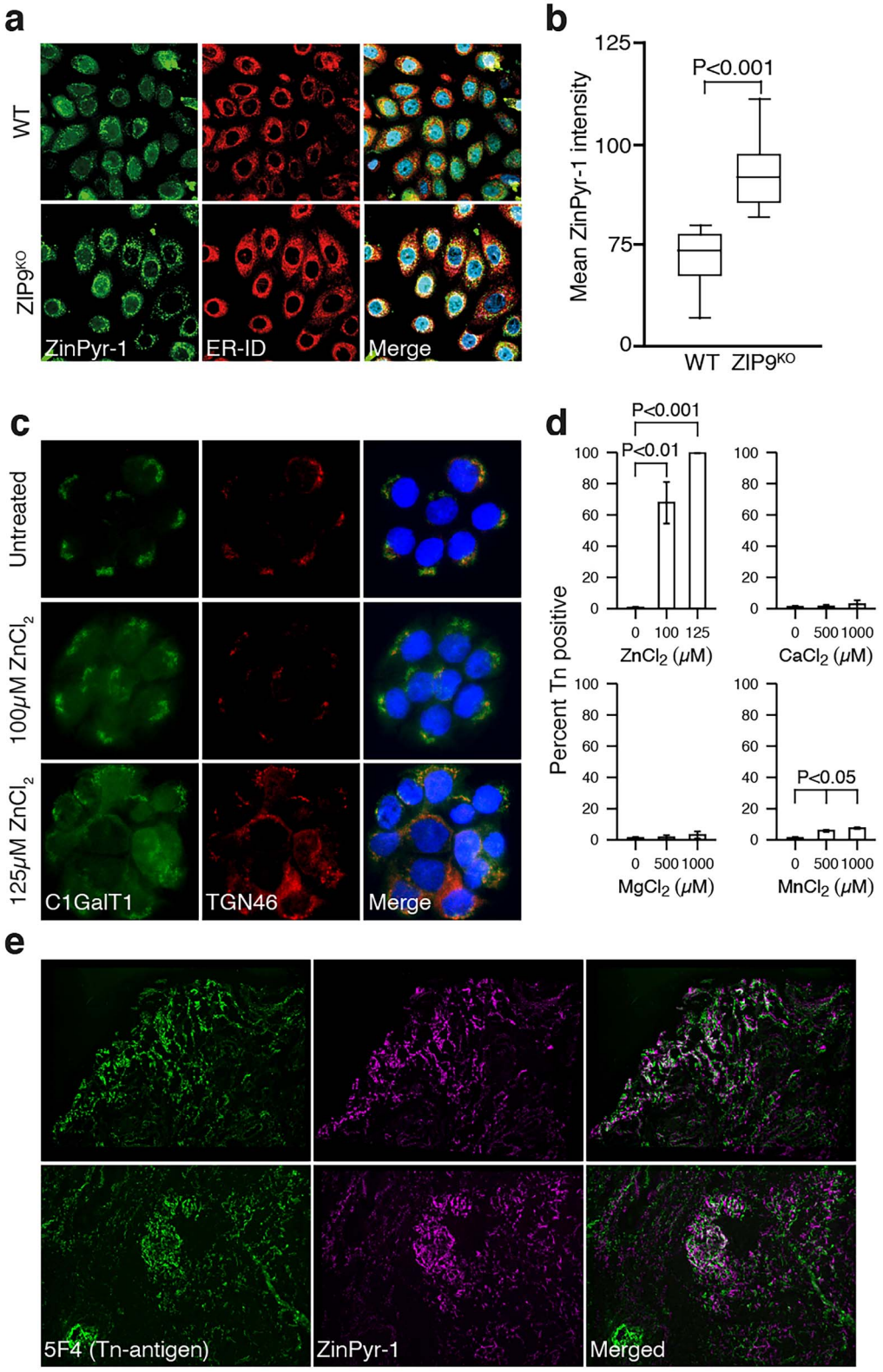

Fig. 6. Examination of the involvement of zinc in the expression of truncated *O*-glycans. a) Immunostaining of N/TERT-1 wildtype (WT) or ZIP9 knockout cells using the ZinPyr-1 zinc-probe or ER-ID. b) ZipPyr-1 intensity was quantified and calculated in Zen Blue (n = 20–50 cells/group). c) Immunostaining of N/TERT-1 wildtype (WT) untreated or treated with 100 μM or 125-μM $ZnCl_2$ for CtGalT1 and TGN46. d) Graphic depiction of the percent of Tn-positive cells, as determined by the intensity of a 5F4 staining using flow cytometry, following treatment with CaCl2, MgCl2, MnCl2, and ZnCl2 divalent cations at various concentrations. Bars illustrate mean percentage, errorbars illustrate the standard deviation, and statistical significance (Student's t-test) is shown where relevant (n = 3). e) Immunostaining of oral squamous cell carcinomas using 5F4 (green) and ZinPyr-1 (magenta) on individual serial sections. The same area of the 2 serial sections was overlaid using ImageJ.

effects of ZIP9 on *O*-glycosylation is partially dependent on C1GalT1 expression secondary to effects on its chaperone, COSMC, most likely in a Zn^{2+} dependent manner (Hanes et al. 2017). We show that ZIP9 knockout results in the accumulation of Zn^{2+} in the secretory pathway. By increasing the concentration of Zn^{2+} in the extracellular environment, we observe an increased expression of Tn in a similar manner to ZIP9 knockout. Even though increased extracellular Zn^{2+} might affect the zinc levels of the secretory pathway, the experiment does not mimic ZIP9 knockout effects exactly, as we experimentally increase extracellular zinc and not only the zinc levels in the secretory pathway. However, as we also observed co-localization of zinc accumulation and Tn-expression in oral squamous cell carcinomas, there seem to be an interplay between truncation of *O*-linked glycans and Zn^{2+} levels. Indeed, several studies have shown that androgen-driven cancer development is driven through ZIP9 dependent processes and that Zn^{2+} is often dysregulated in cancer, suggesting that dysregulated Zn^{2+} homeostasis might affect cancer progression (Münnich et al. 2016; Bulldan et al. 2018; Aguirre-Portolés et al. 2021). Simultaneous investigations of ZIP9 function and glycosylation in cancers has, to the best of our knowledge, not been undertaken.

Our results concur with previous studies by Cummings et al. showing that the oligomerization and activity of the C1GalT1's chaperone COSMC seems to be regulated by Zinc (Hanes et al. 2017). In agreement with this, we observe a downregulation of C1GalT1 in ZIP9 knockout cells. Of note, this downregulation was observed on protein level, not on mRNA-level, indicating alterations to the regulation of C1GalT1 translation or stability. Over-expression of COSMC in ZIP9 knockout cells rescued this phenotype and reduced expression of the Tn-antigen, indicating that C1GalT1 downregulation in ZIP9 knockout cells is dependent on dysfunctional COSMC. COSMC contains a discrete zinc-binding domain (Hanes et al. 2017), and to test if the domain might play a role, we overexpressed a COSMC variant harboring a mutation (E152K) affecting Zn^{2+}-binding (Hanes et al. 2017). However, no difference between the wild type and mutant constructs was found, suggesting that the Zn^{2+} binding domain is not at play in this setting, or over-expression overcomes any reduced activity induced by the E152K mutation. Although downregulation of C1GalT1 provides an explanation as to why we see increased expression of Tn and STn on the cell surface in ZIP9 knockout cells, it does not account for the complete loss of core 2 structures observed in the cells. Synthesis of core 2 structures is regulated by the genes *GCNT1* and *GCNT4*, and the expression of both genes was unaltered as evaluated by RT-qPCR. An alternative and simple explanation for the loss of core 2 structures would be that downregulation of the prerequisite precursor, core 1, but to further explain the complete loss of core 2, protein expression, and the Zn^{2+} dependency of the core 2 synthases should be investigated in depth.

The observed increase in hybrid-type *N*-glycosylation could be caused by an impairment of mannosidase II function, which would prevent the hydrolysis of high-mannose structures to facilitate further modifications of *N*-glycans. However, protein expression of MAN2A2 and mRNA levels of MAN2A1 and MAN2A2 were unaffected by the knockout. It is possible that excess zinc acts on mannosidases via a different mechanism, since zinc-binding sites are situated on the active site of mannosidase II while the sites on COSMC could be on dimerization domains (van den Elsen et al. 2001; Kuntz et al. 2006). An alternative hypothesis is that the increase in hybrid-type *N*-glycans might also be an effect of the hypersialylation of these structures, potentially affecting the trimming to complex-type *N*-glycans. Regarding the mechanism of altered sialylation, androgen-signaling has been shown to affect sialylation in cancer and previous studies have shown that ZIP9 acts as an androgen receptor (Julien et al. 2011), suggesting a potential link between steroid signaling and sialylation through ZIP9. The significant increase in Sec23b could indicate an upregulation in anterograde vesicular transport in the ZIP9 knockout cells, which could suggest a change in the transport of the secretory pathway that may affect the processing of glycans and presentation of glycoproteins or GSLs. In line with this, it has been suggested that re-localization of initiating GALNT enzymes is involved in aberrant *O*-glycosylation in cancer (Gill et al. 2010, 2011; Bard and Chia 2016), and it could therefore be speculated whether the global change in glycosylation observed in our study could be the result of re-localization of select glycosyltransferases. However, knockout of ZIP9 does not affect the general morphology, and the mechanism by which ZIP9 affect core 2 *O*-glycosylation and *N*-glycosylation remains uncovered.

Limitations of the study included the fact that a total of 0.05% of the cells in the first FACS were positive for Tn and/or STn, suggesting that an upwards of 10 gene knockouts should have resulted in expression of truncated *O*-glycans (of which we identify only 3). However, it has previously been shown that cells deficient in elongated *O*-glycans exhibit increased proliferation rates and these cells could therefore be over-represented in the library-transduced cell pool prior to FACS (Radhakrishnan et al. 2014). Furthermore, the massive subsampling of the library and continued passaging could potentially increase the risk of sporadic enrichment of individual sgRNAs. However, only *SLC39A9* (ZIP9), *C1GALT1* (C1GalT1), and *C1GALT1C1* (COSMC) were targeted by more than one sgRNA. Considering the large differences in SigmaFC scores between the identified targets and the next-best targets, we do not consider the strong sampling as a critical issue.

In conclusion, our study is the first unbiased, positive-selection whole-genome CRISPR screen to investigate genes specifically linked to Tn- and STn-expression. We identify knockout of *SLC39A9* (ZIP9), *C1GALT1* (C1GalT1), and *C1GALT1C1* (COSMC) to selectively induce expression of truncated *O*-glycans. Disruption of ZIP9 results in expression of Tn and STn *O*-glycans, obliteration of core 2 *O*-glycans, downregulation of C1GalT1, increased *N*-glycan sialylation, and downregulation of multi-antennary *N*-glycans. Secretory pathway morphology is not strongly affected, but shows accumulation of Zn^{2+} in ZIP9 knockout. Furthermore, we show that Zn^{2+} induces Tn-expression in vitro and that Zn^{2+} accumulation coincides with Tn-expression in tumor tissue. Taken together, these findings show that dysregulation of ZIP9 and Zn^{2+} induce cancer-like glycosylation on the cell surface and suggest that the effect on *O*-glycans is mediated by a downregulation of COSMC.

Materials and methods

Cell culture

HaCaT cells were grown in Dulbecco's modified Eagle medium (DMEM; Gibco, Thermo Fischer Scientific)

supplemented with 10% (vol/vol) heat-inactivated FCS (HyClone), 100-IU/mL penicillin, and 100-μg/mL streptomycin (Gibco, Thermo Fischer Scientific). HEK293T cells were grown in DMEM supplemented with 10% (vol/vol) heat-inactivated fetal bovine serum (FBS; Sigma Aldrich).

N/TERT-1 immortalized keratinocytes (Obtained from JG Rheinwalds lab, Harvard Institute of Medicine, Brigham & Womens Hospital) were cultured in keratinocyte serum-free medium (Gibco, Thermo Fischer Scientific) with 1.25-mg bovine pituitary extract per 500-mL medium (Gibco, Thermo Fischer Scientific), 0.2-ng/mL epidermal growth factor (EGF; Thermo Fischer Scientific), and $CaCl_2$ (Sigma Aldrich) to a final Ca^{2+} concentration of 0.3 mmol/L.

Generation of HaCaT cell lines with constitutive Cas9 expression

Lentiviral vectors were produced in HEK293T cells seeded 72 h prior to transfection at 1×10^5/well density in a 6 well plate and grown until 80–90% confluency. Prior to transfection, HEK293T was grown in DMEM containing 10% FBS without antibiotics. The transfection agent polyethylenimine (PEI; Sigma Aldrich) was prepared at 1 mg/mL as described by the manufacturer. For transfection, 200-μL OPTI-MEM (Gibco, Thermo Fischer Scientific), 8 μL of PEI-stock-solution (1 mg/mL), 0.8-μg lenti-Cas9-Blast (Addgene #52,962), 0.6-μg pCMV-VSV-G (Addgene #8,452), and 0.6-μg psPAX2 (Addgene #12,260) were mixed and incubated for 10 min at room-temperature before added to the adherent HEK293T cells. After 24 h, the transfection medium was replaced by DMEM containing HyClone FCS for HaCaT transduction. Virus-containing supernatant was collected 48 h post-transfection, i.e. when virus had accumulated for 24 h after media change, filtered (0.45 μm) and mixed 1:1 with HyClone FBS containing DMEM and 1:1,000 Polybrene (Sigma Aldrich). HaCaT cells were transduced using 1:1 of medium and virus-containing media overnight. Selection started 48–96 h after transduction, with 5-μg/mL blasticidin S (Gibco, Thermo Fishcer Scientific) for 2 × 4 days including biweekly cell passaging. Cells were harvested and seeded at a concentration of 1 cell/well in 96 well plates. After doubling to sufficient confluency cells were harvested, split 2× into 6 well plates and one well was transduced with a lentiviral preparation of lentiGuide-puro expressing a sgRNA targeting *MS4A1* (CD20; Thomsen et al. 2020). The indel formation at the targeted site was evaluated by IDAA, as described previously (Lonowski et al. 2017). Several cells showed Cas9 activity, of which the cell line 1B6B was isolated by single cell passaging and used for further experiments.

Production of lentiviral vectors for CRISPR screen

The CRISPR screen was conducted using the Brunello library, developed by the Doench laboratory and received through AddGene as a 2-vector system (Pooled Library #73,178) (Doench et al. 2016).

The library was amplified in Lucigen Endura electrocompetent *Escherichia coli* bacteria. 25 μL of bacteria was electroporated with 2 μL of plasmid at voltage of 1,800 V, capacitance of 10, resistance of 600 ohm and a cuvette gap of 0.1 cm. Bacteria was incubated in 1 mL of SOC media and incubated for 1 h at 37 °C, spun down at 2,750 RPM for 5 min, resuspended in 800 μL of SOC media and platted on 20 ampicillin containing agar plates incubated at 37 °C for 14 h. Bacteria was pooled in LB media and subsequently, plasmids were isolated using MIDI prep (Nucleobond).

1×10^7 HEK293T cells per flask were platted in 20 T175 flasks 1 day prior to transfection. Media was changed 1-h prior to transfection. For transfection, 48.2 mL of OPTI-MEM (Gibco, Thermo Fischer Scientific), 1.9 mL of PEI-stock-solution (1 mg/mL), 193.6 μg of Pooled Brunello Library plasmids, 193.6 μg of pCMV-VSV-G (Addgene #8,452), and 193.6 μg of psPAX2 (Addgene #12,260) were mixed and incubated for 10 min at room-temperature and 2.42 mL of the mix was added to each HEK293T containing T175 flask. The day after, media was changed. The following day, media was replaced with 25-mL HyClone FBS containing DMEM. After 24 h, the media was harvested, filtered (0.45 μm) and frozen at −80 °C.

Lentiviral titer was determined by seeding 3×10^4 HaCaT cells/well in two 6-well plates. The subsequent day, 10-mL virus-containing DMEM media with 2 μL of polybrene was added to HaCaT cells in duplications at dilutions of 1:10, 1:100, 1:10,00, 1:10,000, and 1:100,000 with 2 wells serving as negative controls. The next day, media was changed and the following day, selection with 1 μg/mL of puromycin was initiated for 2 × 3 days. After selection, cells were fixed with methanol and stained with crystal violet. Colonies were counted and the titer was determined to 5.8×10^6 CFU/mL.

CRISPR whole-genome knockout screen

8×10^8 HaCaT 1B6B cells were plated in 33 T175 flasks +2 flasks for control counting 24 h prior to transduction. One flask was harvested, and cell numbers determined to ensure proper multiplicity of infection (MOI). Transduction was performed with 2-mL virus-containing media, 18-mL DMEM +10% FBS, and 20-μL polybrene per T175 flask, ensuring transfection at a MOI of 0.25 and a coverage of 500 cells infected per guide in the Brunello library. The day after transfection, media was changed. The subsequent day, selection with media containing 1 μg/mL of puromycin was initiated. Selection was conducted for 2 × 3 days with biweekly passaging of cells, and complete death of negative controls was ensured before selection termination. After selection, cells were harvested by mechanical scraping. 3.6×10^7 cells were spun down and frozen for later DNA extraction and pre-enrichment analysis. The remaining cells were taken for sorting by FACS.

Fluorescence-activated cell sorting

Fluorescence-activated cell sorting (FACS) protocols were first optimized on HaCaT WT cells and HaCaT COSMC knockout cells, generated as previously described (Radhakrishnan et al. 2014). HaCaT WT (Tn-negative) and HaCaT COSMC knockout cells (Tn-positive) were cultured as described, mechanically scraped and mixed at ratios 1:1,000, 1:10,000, and 1:100,000 (COSMC:WT). Cells were suspended in 5F4 (HB-Tn, anti-Tn, and IgM) and 3F1 (HB-STn, anti-STn, and IgG1) antibody-containing supernatant at a density of 10^7 cells/mL and incubated on a rotating stand for 1 h at 4 °C. 5F4 and 3F1 antibodies were produced from hybridoma cells in our own laboratory and have been thoroughly characterized (Clausen et al. 1988; Thurnher et al. 1993; Madsen et al. 2013). Cells were then washed 3× using PBS + 1% bovine serum albumin (BSA). Cells were resuspended in secondary antibody (Dako-0261) diluted in PBS + 1% BSA at 2 ug/mL

for 1 h in darkness at 4 °C on a rotating stand. Cells were then washed 3× using PBS + 1% BSA and sorted using a 488-nm filter on a SONY SH800 FACS (Sony). Thresholds were determined as to ensure sorting in accordance with the mixed ratio of WT vs. COSMC knockout cells and sorting was performed in ultra-purity mode. The same experimental setup and thresholds were used for sorting of cells after performance of CRISPR whole-genome knockout screen as described previously. After FACS of CRISPR whole-genome screened cells, the positive cell population was captured in 15-mL falcon tubes and expanded to a minimum of 4×10^7 cells using cell culture techniques as described previously. The population was split in 2 equally sized samples. These samples underwent FACS as described previously, this time using only the 5F4 or the 3F1 antibody. Cells were expanded to a minimum of 4×10^7 cells prior to NGS.

NGS and bioinformatic analysis

DNA extraction and polymerase chain reaction (PCR) was performed as described by Doench et al using primers as listed (Supplementary Table I; Doench et al. 2016). PCR was purified using AMPure XP according to manufacturer's instruction. The purified product was QC controlled on a Bio-Analyzer according to manufacturer's instructions. Sequencing was performed using Illumina MiSeqV2 with paired-end sequencing at read length of 250 bp using 5% PhiX as spike-in control. Sequencing data were analyzed using the PinAPL-Py software (version 2020/2; Spahn et al. 2017).

Generation of knockout cell lines

Knockout cell lines of ZIP9 were created in both HaCaT and N/TERT-1 cells using a similar methodology as described in section "Generation of HaCaT cell line with constitutive Cas9 expression." However, lenti-Cas9-Blast was replaced by the LentiCRISPR-V2-puro plasmid (Addgene # 52,961), carrying Cas9 and gene specific sgRNAs and selection was performed using puromycin at 1 μg/mL. Guides were cloned and inserted into the LentiCRISPR-V2 vector as described by Ran et al. using oligos as listed (TAGC, Copenhagen; Supplementary Table II; Ran et al. 2013). After transduction and selection, single clones were obtained by serial dilution in 96 well plates and KO clones identified by IDAA using ABI3010/3500 sequenator (ABI/Life Technologies) and Sanger sequencing (GATC, Germany) using primers as listed (Supplementary Table II) and method described previously (Lonowski et al. 2017). A minimum of 2 were selected for each gene with out-of-frame indel formation. IDAA results were analyzed using Peak Scanner Software V1.0 (ABI/Life Technologies).

Immunostaining and microscopy

Cells were cultured on sterile coverslips (Thermo Fischer Scientific). Cells were fixed with acetone, acetone/methanol, or 4% paraformaldehyde (PFA), washed and incubated with primary antibody or PBS as control at 4 °C overnight, washed and incubated with secondary, Alexa Fluor-488 or -594 conjugated antibodies (Invitrogen, Thermo Fischer Scientific) at room-temperature for 45 min. After washing, cells were mounted using ProLong Gold Antifade Reagent with DAPI (Molecular Probes, Thermo Scientific, EU). For lectin staining, a similar protocol was used—however, primary incubation was performed for 30 min at room-temperature at concentrations of 20 μg/mL with biotinylated lectins (Vector labs) and secondary incubation was performed with streptavidin-Alexa Fluor 488 conjugate diluted in PBS with 2.5% BSA to 2 μg/mL. To stain intracellular Zn^{2+}, we incubated live cells with 10 μM of Zinpyr-1 (SantaCruz Biotech CAS 288574-78-7) and contrasted with ER-ID (Enzo Life Sciences ENZ-51026-K500) for 20–30 min at 37 °C in serum-free media. Frozen tissue sections were fixated in ice-cold acetone/methanol for 5 min and stained for 10 min in a 10 μM ZinPyr-1 solution. Excess ZinPyr-1 was removed and sections were mounted as described earlier. Cells were then imaged using either standard fluorescence microscope or high-resolution confocal microscope Zeiss LSM980.

N-, *O*-, and GSL-profiling by MS

N/TERT-1 total cell lysate protein and lipid glycans were released and analyzed by liquid chromatography-tandem mass spectrometry (LC–MS/MS) as described previously (Zhang et al. 2020; de Haan et al. 2022). Briefly, N/TERT-1 cells were grown to 80% confluency and the medium was shifted to 1:1 vol/vol (keratinocyte serum-free medium) K-SFM/DF-K (DMEM/F12) supplemented with 25-μg/mL BPE, 0.2-ng/mL EGF, and 2-mM L-glutamine (Thermo Scientific). After cell culture, the cells were washed once with 5-mL ice-cold PBS and harvested by scraping in 2× 200-μL PBS, followed by centrifugation for 10 min at 600 × *g* and removal of the supernatant. All cell pellets were stored at −80 °C until resuspension in lysis buffer ($\sim 5 \times 10^5$ cells/25 μL).

Twenty-five microliter of each sample was loaded on a PVDF membrane in 96-well plate format and *N*-glycans were released using PNGase F, eluted, and dried. Sialic acids were derivatized by ethyl esterification (α2,6-linked sialic acids) for 0.5 h at 37 °C and subsequent ammonia amidation (α2,3-linked sialic acids) for 0.5 h at 37 °C as described previously and purified by hydrophilic interaction liquid chromatography (HILIC) solid phase extraction (SPE; Selman et al. 2011; Lageveen-Kammeijer et al. 2019). Fifty microliter 2-AB reagent (500-mM 2-AB, 116-mM PB in 45:45:10 metanol:water:acetic acid) was added and the samples were incubated 2.5 h at 50 °C, the glycans were purified by HILIC SPE and eluted in 50-μL water. Ten microliter of the eluates was diluted in 10-μL water for MS analysis.

O-glycans were released from the same samples using 20% hydroxylamine and 20% 1,8-diazabicyclo(5.4.0)undec-7-ene for 1 h at 37 °C, enriched by hydrazide beads, 2-AB labeled as described previously and purified by HILIC and porous graphitic carbon (PGC) SPE. Samples were resolved in 20 μL water and 2 μL of each sample was injected on a nano-flow liquid chromatography (nanoLC) analytical column packed with Reprosil-Pure-AQ C18 phase (Dr. Maisch, 1.9-μm particle size, 15–17-cm column length) using a PicoFrit Emitter (New Objectives, 75-μm inner diameter). The emitter was interfaced to an Orbitrap Fusion Lumos MS (Thermo Fisher Scientific) via a nanoSpray Flex ion source. Samples were eluted in an 1-h method with a gradient from 3% to 32% of solvent B in 35 min, from 32% to 100% B in the next 10 min, and 100% B for the last 15 min at 200 nL/min (solvent A: 0.1% formic acid in water; solvent B: 0.1% formic acid in 80% ACN). A precursor MS scan (*m/z* 200–1,700, positive polarity) was acquired in the Orbitrap at a nominal resolution of 120,000, followed by Orbitrap HCD-MS/MS at a nominal resolution of 50,000 of the 10 most abundant precursors

in the MS spectrum (charge states 1–4). A minimum MS signal threshold of 30,000 was used to trigger data-dependent fragmentation events. HCD was performed with an energy of 27% ± 5%, applying a 20-s dynamic exclusion window. Extraction of GSL and analysis of GSL-glycan alditols were performed in triplicate as previously described (Zhang et al. 2020, 2022). In brief, GSLs were extracted and purified from ~1 × 10^6 cells. GSL-glycan was enzymatically released by EGCase I for 36 h at 37 °C. The released glycans were collected and purified by C18 SPE followed by reduction using 20 μL of sodium borohydride (500 mM) in potassium hydroxide (50 mM). Subsequently, GSL-glycans were desalted by cation exchange SPE and further purified by PGC SPE. The purified glycan alditols were resuspended in 20 μL of water prior to PGC nano-LC–ESI–MS/MS analysis in negative-ion mode. MS spectra were acquired within an *m/z* range of 340–1,850 for GSL-glycans in enhanced mode using smart parameter setting (SPS) was set to *m/z* 900. Glycan structures were assigned on the basis of the known MS/MS fragmentation patterns in negative-ion mode (Anugraham et al. 2015; Zhang et al. 2020, 2022), elution order, and general glycobiological knowledge. Data analyses and structural annotation were performed as described previously (de Haan et al. 2022). *N*-, *O*-, and GSL-glycans were relatively quantified separately, by total area normalization. Derived traits were calculated based on specific glycosylation features, including fucosylation, sialylation, glycan type, and antennarity for *N*-glycans, whereas for *O*-GalNAc glycans the relative abundance of the different cores was determined.

RT-qPCR

RNA was isolated from cell pellets using the RNeasy Micro kit (QIAGEN) according to manufacturer's instructions, followed by reverse transcription using the Maxima First Strand cDNA Synthesis Kit (Thermo Scientific), loading 1-μg RNA/sample. Relevant primers, cDNA and LightCycler 480 SYBR Green I Master (Roche) was mixed and quantitative PCR was performed using a 2-step protocol with a 60 °C, 1-min annealing-elongation step and a 95 °C, 30-s denaturation step in 40 cycles on a LightCycler 480 instrument (Roche). Cp values were extracted using the Absolute quantification/2nd derivative max method. All samples were evaluated in 2 technical replicates, and the average of these used to analyze the data according to the ΔΔCp method.

Abbreviations

BSA: bovine serum albumin
DMEM: Dulbecco's modified Eagle medium
FACS: fluorescence-activated cell sorting
FBS: fetal bovine serum
GSL: glycosphingolipid
HILIC: hydrophilic interaction liquid chromatography
IDAA: indel detection by amplicon analysis
K-SFM: keratinocyte serum-free medium
MOI: multiplicity of infection
MS: mass spectrometry
nanoLC: nano-flow liquid chromatography
NGS: next generation sequencing
PCR: polymerase chain reaction
PFA: paraformaldehyde
PGC: porous graphitic carbon
SPE: solid phase extraction
STn-antigen: Sialyl-Tn antigen
Tn antigen: Thomson-nouveau antigen

Acknowledgments

We are grateful to the lab of John Doench at Broad Institute, from whom the Brunello library was received as a generous gift donated through AddGene. We further thank Mette Juul Jacobsen and Lasse Vinner from the National High-Throughput DNA Sequencing Center, Copenhagen, for NGS assistance. The PinAPL-Py software was developed by the Lewis, Harismendy and Esko laboratories, whom we would also like to thank.

Credit for author contributions

Troels Boldt Rømer and Hans H. Wandall with assistance from Emil Marek Heymans Pallesen, Mikkel Koed Møller Aasted, Fawzi Khoder-Agha, August Dylander, Emil Aagaard Thomsen, and Jacob Giehm Mikkelsen (Conceptualization and design), Troels Boldt Rømer, August Dylander, Sabrina Horn, Mikkel Koed Møller Aasted, Noortje de Haan, Fawzi Khoder-Agha, Emil Marek Heymans Pallesen, Manfred Wuhrer, Tao Zhang, and Sally Dabelsteen (Experiments), Troels Boldt Rømer (Bioinformatics/CRISPR-screen), Noortje de Haan, Troels Boldt Rømer, Mikkel Koed Møller Aasted, Fawzi Khoder-Agha, August Dylander, and Hans H. Wandall (Data analysis and validation). Troels Boldt Rømer and Hans H. Wandall (Writing—original draft). All authors (Writing—review & editing).

Supplementary material

Supplementary material is available at *Glycobiology Journal* online.

Funding

This work was supported by the Danish Cancer Society and the University of Copenhagen Faculty of Health and Medical Sciences; the European Research Council (ERC) under the European Union's Horizon 2020 research and innovation program (GlycoSkin H2020-ERC; 772735); Remodel; the NEYE Foundation; the LUNDBECK foundation; and the Independent Research Fund Denmark Medical Sciences (9039-00173B).

Conflict of interest statement: H.H.W. owns stocks and is a consultant for and co-founder of EbuMab, ApS. And GO-Therapeutics, Inc. H.H.W. and M.K.M.A. are co-inventors of a novel antibody targeting truncated *O*-glycans. The remaining authors declare no competing interests.

Data availability

All data included in the study is available upon request to the corresponding author.

Ethics approval and consent to participate

Informed consent was obtained from all subjects, and the study was conducted in accordance with the Declaration of Helsinki.

References

Aguirre-Portolés C, Payne R, Trautz A, Foskett JK, Natale CA, Seykora JT, Ridky TW. ZIP9 is a druggable determinant of sex

differences in melanoma. *Cancer Res*. 2021:**81**(23):5991–6003. doi: https://doi.org/10.1158/0008-5472.CAN-21-0982.

Anugraham M, Everest-Dass AV, Jacob F, Packer NH. A platform for the structural characterization of glycans enzymatically released from glycosphingolipids extracted from tissue and cells. *Rapid Commun Mass Spectrom RCM*. 2015:**29**(7):545–561. doi: https://doi.org/10.1002/rcm.7130.

Axelsson MA, Karlsson NG, Steel DM, Ouwendijk J, Nilsson T, Hansson GC. Neutralization of pH in the Golgi apparatus causes redistribution of glycosyltransferases and changes in the O-glycosylation of mucins. *Glycobiology*. 2001:**11**(8):633–644. doi: https://doi.org/10.1093/glycob/11.8.633.

Bard F, Chia J. Cracking the glycome encoder: signaling, trafficking, and glycosylation. *Trends Cell Biol*. 2016:**26**(5):379–388. doi: https://doi.org/10.1016/j.tcb.2015.12.004.

Bennett EP, Mandel U, Clausen H, Gerken TA, Fritz TA, Tabak LA. Control of mucin-type O-glycosylation: a classification of the polypeptide GalNAc-transferase gene family. *Glycobiology*. 2012:**22**(6):736–756. doi: https://doi.org/10.1093/glycob/cwr182.

Bhide GP, Colley KJ. Sialylation of N-glycans: mechanism, cellular compartmentalization and function. *Histochem Cell Biol*. 2017:**147**(2):149–174. doi: https://doi.org/10.1007/s00418-016-1520-x.

Blanas A, Sahasrabudhe NM, Rodríguez E, van Kooyk Y, van Vliet SJ. Fucosylated antigens in cancer: an alliance toward tumor progression, metastasis, and resistance to chemotherapy. *Front Oncol*. 2018:**8**:39. doi: https://doi.org/10.3389/fonc.2018.00039.

Boyaval F, Van Zeijl R, Dalebout H, Holst S, van Pelt G, Fariña-Sarasqueta A, Mesker W, Tollenaar R, Morreau H, Wuhrer M, et al. N-glycomic signature of stage II colorectal cancer and its association with the tumor microenvironment. *Mol Cell Proteomics MCP*. 2021:**20**:100057–100057. doi: https://doi.org/10.1074/mcp.RA120.002215.

Brockhausen I, Stanley P. 2015. O-GalNAc Glycans. In: Varki A, Cummings RD, Esko JD, Stanley P, Hart GW, Aebi M, Darvill AG, Kinoshita T, Packer NH, Prestegard JH, et al., editors. *Essentials of glycobiology*. 3rd ed. Cold Spring Harbor (NY): Cold Spring Harbor Laboratory Press. [accessed 2020 Mar 23]. http://www.ncbi.nlm.nih.gov/books/NBK453030/.

Büll C, Stoel MA, den Brok MH, Adema GJ. Sialic acids sweeten a tumor's life. *Cancer Res*. 2014:**74**(12):3199–3204. doi: https://doi.org/10.1158/0008-5472.CAN-14-0728.

Bulldan A, Bartsch J-W, Konrad L, Scheiner-Bobis G. ZIP9 but not the androgen receptor mediates testosterone-induced migratory activity of metastatic prostate cancer cells. *Biochim Biophys Acta Mol Cell Res*. 2018:**1865**(12):1857–1868. doi: https://doi.org/10.1016/j.bbamcr.2018.09.004.

Cervoni GE, Cheng JJ, Stackhouse KA, Heimburg-Molinaro J, Cummings RD. O-glycan recognition and function in mice and human cancers. *Biochem J*. 2020:**477**(8):1541–1564. doi: https://doi.org/10.1042/BCJ20180103.

Chia J, Goh G, Bard F. Short O-GalNAc glycans: regulation and role in tumor development and clinical perspectives. *Biochim Biophys Acta*. 2016:**1860**(8):1623–1639. doi: https://doi.org/10.1016/j.bbagen.2016.03.008.

Chiodo F, de Haas A, van Vliet SJ, van Kooyk Y. 2021. Human C-type lectins, MGL, DC-SIGN and Langerin, their interactions with endogenous and exogenous ligand patterns. In: *Comprehensive glycoscience*. Amsterdam, Netherlands: Elsevier. p. 425–441. [accessed 2022 Jul 5]. https://linkinghub.elsevier.com/retrieve/pii/B9780128194751000900.

Clausen H, Stroud M, Parker J, Springer G, Hakomori S. Monoclonal antibodies directed to the blood group A associated structure, galactosyl-A: specificity and relation to the Thomsen-Friedenreich antigen. *Mol Immunol*. 1988:**25**(2):199–204. doi: https://doi.org/10.1016/0161-5890(88)90068-5.

Converse A, Thomas P. 2020. The zinc transporter ZIP9 (Slc39a9) regulates zinc dynamics essential to egg activation in zebrafish. *Sci Rep* **10**. doi: https://doi.org/10.1038/s41598-020-72515-4. [accessed 2021 Mar 11]. https://www.ncbi.nlm.nih.gov/pmc/articles/PMC7518430/.

Coon JS, Weinstein RS, Summers JL. Blood group precursor T-antigen expression in human urinary bladder carcinoma. *Am J Clin Pathol*. 1982:**77**(6):692–699. doi: https://doi.org/10.1093/ajcp/77.6.692.

Crocker PR, Paulson JC, Varki A. Siglecs and their roles in the immune system. *Nat Rev Immunol*. 2007:**7**(4):255–266. doi: https://doi.org/10.1038/nri2056.

DeNicola GM, Chen P-H, Mullarky E, Sudderth JA, Hu Z, Wu D, Tang H, Xie Y, Asara JM, Huffman KE, et al. NRF2 regulates serine biosynthesis in non–small cell lung cancer. *Nat Genet*. 2015:**47**(12):1475–1481. doi: https://doi.org/10.1038/ng.3421.

Dennis JW, Laferté S, Waghorne C, Breitman ML, Kerbel RS. Beta 1-6 branching of Asn-linked oligosaccharides is directly associated with metastasis. *Science*. 1987:**236**(4801):582–585. doi: https://doi.org/10.1126/science.2953071.

Desai PR. Immunoreactive T and Tn antigens in malignancy: role in carcinoma diagnosis, prognosis, and immunotherapy. *Transfus Med Rev*. 2000:**14**(4):312–325. doi: https://doi.org/10.1053/tmrv.2000.16229.

Doench JG, Fusi N, Sullender M, Hegde M, Vaimberg EW, Donovan KF, Smith I, Tothova Z, Wilen C, Orchard R, et al. Optimized sgRNA design to maximize activity and minimize off-target effects of CRISPR-Cas9. *Nat Biotechnol*. 2016:**34**(2):184–191. doi: https://doi.org/10.1038/nbt.3437.

Doherty M, Theodoratou E, Walsh I, Adamczyk B, Stöckmann H, Agakov F, Timofeeva M, Trbojević-Akmačić I, Vučković F, Duffy F, et al. Plasma N-glycans in colorectal cancer risk. *Sci Rep*. 2018:**8**(1):8655. doi: https://doi.org/10.1038/s41598-018-26805-7.

van den Elsen JMH, Kuntz DA, Rose DR. Structure of Golgi α-mannosidase II: a target for inhibition of growth and metastasis of cancer cells. *EMBO J*. 2001:**20**(12):3008–3017. doi: https://doi.org/10.1093/emboj/20.12.3008.

Evers B, Jastrzebski K, Heijmans JPM, Grernrum W, Beijersbergen RL, Bernards R. CRISPR knockout screening outperforms shRNA and CRISPRi in identifying essential genes. *Nat Biotechnol*. 2016:**34**(6):631–633. doi: https://doi.org/10.1038/nbt.3536.

Gao N, Bergstrom K, Fu J, Xie B, Chen W, Xia L. Loss of intestinal O-glycans promotes spontaneous duodenal tumors. *Am J Physiol Gastrointest Liver Physiol*. 2016:**311**(1):G74–G83. doi: https://doi.org/10.1152/ajpgi.00060.2016.

Gill DJ, Chia J, Senewiratne J, Bard F. Regulation of O-glycosylation through Golgi-to-ER relocation of initiation enzymes. *J Cell Biol*. 2010:**189**(5):843–858. doi: https://doi.org/10.1083/jcb.201003055.

Gill DJ, Clausen H, Bard F. Location, location, location: new insights into O-GalNAc protein glycosylation. *Trends Cell Biol*. 2011:**21**(3):149–158. doi: https://doi.org/10.1016/j.tcb.2010.11.004.

de Haan N, Narimatsu Y, Koed Møller Aasted M, Larsen ISB, Marinova IN, Dabelsteen S, Vakhrushev SY, Wandall HH. In-depth profiling of O-glycan isomers in human cells using C18 nanoliquid chromatography–mass spectrometry and glycogenomics. *Anal Chem*. 2022:**94**(10):4343–4351. doi: https://doi.org/10.1021/acs.analchem.1c05068.

Han J, Perez JT, Chen C, Li Y, Benitez A, Kandasamy M, Lee Y, Andrade J, tenOever B, Manicassamy B. Genome-wide CRISPR/Cas9 screen identifies host factors essential for influenza virus replication. *Cell Rep*. 2018:**23**(2):596–607. doi: https://doi.org/10.1016/j.celrep.2018.03.045.

Hanes MS, Moremen KW, Cummings RD. Biochemical characterization of functional domains of the chaperone Cosmc. *PLoS One*. 2017:**12**(6):e0180242. doi: https://doi.org/10.1371/journal.pone.0180242.

Hanzawa K, Tanaka-Okamoto M, Murakami H, Suzuki N, Mukai M, Takahashi H, Omori T, Ikezawa K, Ohkawa K, Ohue M, et al. Increased levels of acidic free-N-glycans, including multi-antennary and fucosylated structures, in the urine of cancer patients. *PLoS One*. 2022:**17**(4):e0266927. doi: https://doi.org/10.1371/journal.pone.0266927.

Hassinen A, Pujol FM, Kokkonen N, Pieters C, Kihlström M, Korhonen K, Kellokumpu S. Functional organization of Golgi N- and O-glycosylation pathways involves pH-dependent complex formation that is impaired in cancer cells. *J Biol Chem*. 2011:**286**(44): 38329–38340. doi: https://doi.org/10.1074/jbc.M111.277681.

Housden BE, Perrimon N. Comparing CRISPR and RNAi-based screening technologies. *Nat Biotechnol*. 2016:**34**(6):621–623. doi: https://doi.org/10.1038/nbt.3599.

Ju T, Cummings RD. A unique molecular chaperone Cosmc required for activity of the mammalian core 1 beta 3-galactosyltransferase. *Proc Natl Acad Sci U S A*. 2002:**99**(26):16613–16618. doi: https://doi.org/10.1073/pnas.262438199.

Ju T, Cummings RD. 2014. Core 1 β3Galactosyltransferase (C1GalT1, T-synthase) and its specific molecular chaperone Cosmc (C1GalT1C1). In: Taniguchi N, Honke K, Fukuda M, Narimatsu H, Yamaguchi Y, Angata T, editors. *Handbook of glycosyltransferases and related genes*. Tokyo: Springer Japan. p. 149–169. [accessed 2020 Apr 19]. https://doi.org/10.1007/978-4-431-54240-7_65.

Ju T, Lanneau GS, Gautam T, Wang Y, Xia B, Stowell SR, Willard MT, Wang W, Xia JY, Zuna RE, et al. Human tumor antigens Tn and sialyl Tn arise from mutations in Cosmc. *Cancer Res*. 2008:**68**(6):1636–1646. doi: https://doi.org/10.1158/0008-5472.CAN-07-2345.

Ju T, Aryal RP, Kudelka MR, Wang Y, Cummings RD. The Cosmc connection to the Tn antigen in cancer. *Cancer Biomark Sect Dis Markers*. 2014:**14**(1):63–81. doi: https://doi.org/10.3233/CBM-130375.

Julien S, Ivetic A, Grigoriadis A, QiZe D, Burford B, Sproviero D, Picco G, Gillett C, Papp SL, Schaffer L, et al. Selectin ligand Sialyl-Lewis x antigen drives metastasis of hormone-dependent breast cancers. *Cancer Res*. 2011:**71**(24):7683. doi: https://doi.org/10.1158/0008-5472.CAN-11-1139.

Julien S, Videira PA, Delannoy P. Sialyl-tn in cancer: (how) did we miss the target? *Biomol Ther*. 2012:**2**(4):435–466. doi: https://doi.org/10.3390/biom2040435.

King SL, Joshi HJ, Schjoldager KT, Halim A, Madsen TD, Dziegiel MH, Woetmann A, Vakhrushev SY, Wandall HH. Characterizing the O-glycosylation landscape of human plasma, platelets, and endothelial cells. *Blood Adv*. 2017:**1**(7):429–442. doi: https://doi.org/10.1182/bloodadvances.2016002121.

Kobayashi H, Terao T, Kawashima Y. Serum sialyl Tn as an independent predictor of poor prognosis in patients with epithelial ovarian cancer. *J Clin Oncol Off J Am Soc Clin Oncol*. 1992:**10**(1):95–101. doi: https://doi.org/10.1200/JCO.1992.10.1.95.

Kuntz DA, Liu H, Bols M, Rose DR. The role of the active site Zn in the catalytic mechanism of the GH38 Golgi α-mannosidase II: implications from noeuromycin inhibition. *Biocatal Biotransformation*. 2006:**24**(1–2):55–61. doi: https://doi.org/10.1080/10242420500533242.

Lageveen-Kammeijer GSM, de Haan N, Mohaupt P, Wagt S, Filius M, Nouta J, Falck D, Wuhrer M. Highly sensitive CE-ESI-MS analysis of N-glycans from complex biological samples. *Nat Commun*. 2019:**10**(1):2137. doi: https://doi.org/10.1038/s41467-019-09910-7.

Lonowski LA, Narimatsu Y, Riaz A, Delay CE, Yang Z, Niola F, Duda K, Ober EA, Clausen H, Wandall HH, et al. Genome editing using FACS enrichment of nuclease-expressing cells and indel detection by amplicon analysis. *Nat Protoc*. 2017:**12**(3):581–603. doi: https://doi.org/10.1038/nprot.2016.165.

Madsen CB, Petersen C, Lavrsen K, Harndahl M, Buus S, Clausen H, Pedersen AE, Wandall HH. Cancer associated aberrant protein O-glycosylation can modify antigen processing and immune response. *PLoS One*. 2012:**7**(11):e50139. doi: https://doi.org/10.1371/journal.pone.0050139.

Madsen CB, Lavrsen K, Steentoft C, Vester-Christensen MB, Clausen H, Wandall HH, Pedersen AE. Glycan elongation beyond the mucin associated Tn antigen protects tumor cells from immune-mediated killing. *PLoS One*. 2013:**8**(9):e72413. doi: https://doi.org/10.1371/journal.pone.0072413.

Mandel U, Petersen OW, Sørensen H, Vedtofte P, Hakomori S, Clausen H, Dabelsteen E. Simple mucin-type carbohydrates in oral stratified squamous and salivary gland epithelia. *J Invest Dermatol*. 1991:**97**(4):713–721. doi: https://doi.org/10.1111/1523-1747.ep12484064.

Mathiesen CBK, Carlsson MC, Brand S, Möller SR, Idorn M, Thor Straten P, Pedersen AE, Dabelsteen S, Halim A, Würtzen PA, et al. Genetically engineered cell factories produce glycoengineered vaccines that target antigen-presenting cells and reduce antigen-specific T-cell reactivity. *J Allergy Clin Immunol*. 2018:**142**(6):1983–1987. doi: https://doi.org/10.1016/j.jaci.2018.07.030.

Matsuura W, Yamazaki T, Yamaguchi-Iwai Y, Masuda S, Nagao M, Andrews GK, Kambe T. SLC39A9 (ZIP9) regulates zinc homeostasis in the secretory pathway: characterization of the ZIP subfamily I protein in vertebrate cells. *Biosci Biotechnol Biochem*. 2009:**73**(5):1142–1148. doi: https://doi.org/10.1271/bbb.80910.

Mehta A, Norton P, Liang H, Comunale MA, Wang M, Rodemich-Betesh L, Koszycki A, Noda K, Miyoshi E, Block T. Increased levels of tetra-antennary N-linked glycan but not core fucosylation are associated with hepatocellular carcinoma tissue. *Cancer Epidemiol Biomark Prev Publ Am Assoc Cancer Res Cosponsored Am Soc Prev Oncol*. 2012:**21**(6):925–933. doi: https://doi.org/10.1158/1055-9965.EPI-11-1183.

Mereiter S, Balmaña M, Campos D, Gomes J, Reis CA. Glycosylation in the era of cancer-targeted therapy: where are we heading? *Cancer Cell*. 2019:**36**(1):6–16. doi: https://doi.org/10.1016/j.ccell.2019.06.006.

Münnich N, Wernhart S, Hogstrand C, Schlomann U, Nimsky C, Bartsch JW. Expression of the zinc importer protein ZIP9/SLC39A9 in glioblastoma cells affects phosphorylation states of p53 and GSK-3β and causes increased cell migration. *Biometals Int J Role Met Ions Biol Biochem Med*. 2016:**29**(6):995–1004. doi: https://doi.org/10.1007/s10534-016-9971-z.

Nguyen AT, Chia J, Ros M, Hui KM, Saltel F, Bard F. Organelle specific O-glycosylation drives MMP14 activation, tumor growth, and metastasis. *Cancer Cell*. 2017:**32**(5):639–653.e6. doi: https://doi.org/10.1016/j.ccell.2017.10.001.

Park DD, Phoomak C, Xu G, Olney LP, Tran KA, Park SS, Haigh NE, Luxardi G, Lert-Itthiporn W, Shimoda M, et al. Metastasis of cholangiocarcinoma is promoted by extended high-mannose glycans. *Proc Natl Acad Sci U S A*. 2020:**117**(14):7633–7644. doi: https://doi.org/10.1073/pnas.1916498117.

Pinho SS, Reis CA. Glycosylation in cancer: mechanisms and clinical implications. *Nat Rev Cancer*. 2015:**15**(9):540–555. doi: https://doi.org/10.1038/nrc3982.

Posey AD, Schwab RD, Boesteanu AC, Steentoft C, Mandel U, Engels B, Stone JD, Madsen TD, Schreiber K, Haines KM, et al. Engineered CAR T cells targeting the cancer-associated Tn-glycoform of the membrane mucin MUC1 control adenocarcinoma. *Immunity*. 2016:**44**(6):1444–1454. doi: https://doi.org/10.1016/j.immuni.2016.05.014.

Qiu Y, Gao Y, Yu D, Zhong L, Cai W, Ji J, Geng F, Tang G, Zhang H, Cao J, et al. Genome-wide analysis reveals zinc transporter ZIP9 regulated by DNA methylation promotes radiation-induced skin fibrosis via the TGF-β signaling pathway. *J Invest Dermatol*. 2020:**140**(1):94–102.e7. doi: https://doi.org/10.1016/j.jid.2019.04.027.

Radhakrishnan P, Dabelsteen S, Madsen FB, Francavilla C, Kopp KL, Steentoft C, Vakhrushev SY, Olsen JV, Hansen L, Bennett EP, et al. Immature truncated O-glycophenotype of cancer directly induces oncogenic features. *Proc Natl Acad Sci U S A*. 2014:**111**(39):E4066–E4075. doi: https://doi.org/10.1073/pnas.1406619111.

Ran FA, Hsu PD, Wright J, Agarwala V, Scott DA, Zhang F. Genome engineering using the CRISPR-Cas9 system. *Nat Protoc*. 2013:**8**(11): 2281–2308. doi: https://doi.org/10.1038/nprot.2013.143.

Rømer TB, Aasted MKM, Dabelsteen S, Groen A, Schnabel J, Tan E, Pedersen JW, Haue AD, Wandall HH. Mapping of truncated O-glycans in cancers of epithelial and non-epithelial origin. *Br*

J Cancer. 2021:**125**(9):1239–1250. doi: https://doi.org/10.1038/s41416-021-01530-7.

Schietinger A, Philip M, Yoshida BA, Azadi P, Liu H, Meredith SC, Schreiber H. A mutant chaperone converts a wild-type protein into a tumor-specific antigen. *Science*. 2006:**314**(5797):304–308. doi: https://doi.org/10.1126/science.1129200.

Selman MHJ, Hemayatkar M, Deelder AM, Wuhrer M. Cotton HILIC SPE microtips for microscale purification and enrichment of glycans and glycopeptides. *Anal Chem*. 2011:**83**(7):2492–2499. doi: https://doi.org/10.1021/ac1027116.

Shalem O, Sanjana NE, Hartenian E, Shi X, Scott DA, Mikkelsen TS, Heckl D, Ebert BL, Root DE, Doench JG, et al. Genome-scale CRISPR-Cas9 knockout screening in human cells. *Science*. 2014:**343**(6166):84–87. doi: https://doi.org/10.1126/science.1247005.

Spahn PN, Bath T, Weiss RJ, Kim J, Esko JD, Lewis NE, Harismendy O. PinAPL-Py: a comprehensive web-application for the analysis of CRISPR/Cas9 screens. *Sci Rep*. 2017:**7**(1):1–8. doi: https://doi.org/10.1038/s41598-017-16193-9.

Springer GF. Blood group T and Tn antigens are universal, clonal, epithelial cell-adhesive, autoimmunogenic carcinoma markers. *Prog Clin Biol Res*. 1983:**133**:157–166.

Springer GF. T and Tn, general carcinoma autoantigens. *Science*. 1984:**224**(4654):1198–1206. doi: https://doi.org/10.1126/science.6729450.

Springer GF. Immunoreactive T and Tn epitopes in cancer diagnosis, prognosis, and immunotherapy. *J Mol Med Berl Ger*. 1997:**75**(8):594–602. doi: https://doi.org/10.1007/s001090050144.

Steentoft C, Vakhrushev SY, Joshi HJ, Kong Y, Vester-Christensen MB, Schjoldager KT-BG, Lavrsen K, Dabelsteen S, Pedersen NB, Marcos-Silva L, et al. Precision mapping of the human O-GalNAc glycoproteome through SimpleCell technology. *EMBO J*. 2013:**32**(10):1478–1488. doi: https://doi.org/10.1038/emboj.2013.79.

Steentoft C, Migliorini D, King TR, Mandel U, June CH, Posey AD. Glycan-directed CAR-T cells. *Glycobiology*. 2018:**28**(9):656–669. doi: https://doi.org/10.1093/glycob/cwy008.

Stowell SR, Ju T, Cummings RD. Protein glycosylation in cancer. *Annu Rev Pathol*. 2015:**10**:473–510. doi: https://doi.org/10.1146/annurev-pathol-012414-040438.

Sun X, Ju T, Cummings RD. Differential expression of Cosmc, T-synthase and mucins in Tn-positive colorectal cancers. *BMC Cancer*. 2018:**18**. doi: https://doi.org/10.1186/s12885-018-4708-8. [accessed 2020 Feb 11]. https://www.ncbi.nlm.nih.gov/pmc/articles/PMC6097208/.

Thomas P, Pang Y, Dong J, Berg AH. Identification and characterization of membrane androgen receptors in the ZIP9 zinc transporter subfamily: II. Role of human ZIP9 in testosterone-induced prostate and breast cancer cell apoptosis. *Endocrinology*. 2014:**155**(11):4250–4265. doi: https://doi.org/10.1210/en.2014-1201.

Thomas P, Converse A, Berg HA. ZIP9, a novel membrane androgen receptor and zinc transporter protein. *Gen Comp Endocrinol*. 2018:**257**:130–136. doi: https://doi.org/10.1016/j.ygcen.2017.04.016.

Thomsen EA, Rovsing AB, Anderson MV, Due H, Huang J, Luo Y, Dybkaer K, Mikkelsen JG. Identification of BLNK and BTK as mediators of rituximab-induced programmed cell death by CRISPR screens in GCB-subtype diffuse large B-cell lymphoma. *Mol Oncol*. 2020:**14**(9):1978–1997. doi: https://doi.org/10.1002/1878-0261.12753.

Thurnher M, Clausen H, Sharon N, Berger EG. Use of O-glycosylation-defective human lymphoid cell lines and flow cytometry to delineate the specificity of Moluccella laevis lectin and monoclonal antibody 5F4 for the Tn antigen (GalNAc alpha 1-O-Ser/Thr). *Immunol Lett*. 1993:**36**(3):239–243. doi: https://doi.org/10.1016/0165-2478(93)90095-j.

Varki A, Cummings RD, Esko JD, Stanley P, Hart GW, Aebi M, Darvill AG, Kinoshita T, Packer NH, Prestegard JH, et al., editors. 2015. *Essentials of glycobiology*. 3rd ed. Cold Spring Harbor (NY): Cold Spring Harbor Laboratory Press. [accessed 2020 Apr 12]. http://www.ncbi.nlm.nih.gov/books/NBK310274/.

van Vliet SJ, Gringhuis SI, Geijtenbeek TBH, van Kooyk Y. Regulation of effector T cells by antigen-presenting cells via interaction of the C-type lectin MGL with CD45. *Nat Immunol*. 2006:**7**(11):1200–1208. doi: https://doi.org/10.1038/ni1390.

de Vroome SW, Holst S, Girondo MR, van der Burgt YEM, Mesker WE, Tollenaar RAEM, Wuhrer M. Serum N-glycome alterations in colorectal cancer associate with survival. *Oncotarget*. 2018:**9**(55):30610–30623. doi: https://doi.org/10.18632/oncotarget.25753.

Wandall HH, Nielsen MAI, King-Smith S, de Haan N, Bagdonaite I. Global functions of O-glycosylation: promises and challenges in O-glycobiology. *FEBS J*. 2021:**288**(24):7183–7212. doi: https://doi.org/10.1111/febs.16148.

Wang Y, Ju T, Ding X, Xia B, Wang W, Xia L, He M, Cummings RD. Cosmc is an essential chaperone for correct protein O-glycosylation. *Proc Natl Acad Sci U S A*. 2010:**107**(20):9228–9233. doi: https://doi.org/10.1073/pnas.0914004107.

Werther JL, Tatematsu M, Klein R, Kurihara M, Kumagai K, Llorens P, Guidugli Neto J, Bodian C, Pertsemlidis D, Yamachika T, et al. Sialosyl-Tn antigen as a marker of gastric cancer progression: an international study. *Int J Cancer*. 1996:**69**(3):193–199. doi: https://doi.org/10.1002/(SICI)1097-0215(19960621)69:3<193::AID-IJC8>3.0.CO;2-V.

Yamaji T, Hanamatsu H, Sekizuka T, Kuroda M, Iwasaki N, Ohnishi M, Furukawa J-I, Yahiro K, Hanada K. A CRISPR screen using subtilase cytotoxin identifies SLC39A9 as a glycan-regulating factor. *iScience*. 2019:**15**:407–420. doi: https://doi.org/10.1016/j.isci.2019.05.005.

Zhang T, van Die I, Tefsen B, van Vliet SJ, Laan LC, Zhang J, Ten Dijke P, Wuhrer M, Belo AI. Differential O- and glycosphingolipid glycosylation in human pancreatic adenocarcinoma cells with opposite morphology and metastatic behavior. *Front Oncol*. 2020:**10**:732. doi: https://doi.org/10.3389/fonc.2020.00732.

Zhang J, Zhang Z, Holst S, Blöchl C, Madunic K, Wuhrer M, Ten Dijke P, Zhang T. Transforming growth factor-β challenge alters the N-, O-, and glycosphingolipid glycomes in PaTu-S pancreatic adenocarcinoma cells. *J Biol Chem*. 2022:**298**(3):101717. doi: https://doi.org/10.1016/j.jbc.2022.101717.

Zhou Y, Zhu S, Cai C, Yuan P, Li C, Huang Y, Wei W. High-throughput screening of a CRISPR/Cas9 library for functional genomics in human cells. *Nature*. 2014:**509**(7501):487–491. doi: https://doi.org/10.1038/nature13166.